A Geochemical Study of the Carboniferous Audhild Volcanics, Northwestern Ellesmere Island, Arctic Canada: Initial Volcanism in the Sverdrup Basin

by David H. Ritcey

Submitted in Partial Fulfillment of the Requirements

for the Degree of Bachelor of Arts, Honours

Dalhousie University,

Halifax, Nova Scotia

March, 1989

DALHOUSIE UNIVERSITY
Department of Geology
Halifax, N.S. Canada B3H 3J5 Telephone (902) 424-2358 Telex: 019-21863

DALHOUSIE UNIVERSITY, DEPARTMENT OF GEOLOGY

B.A. HONOURS THESIS

Author: David H. Ritcey

Title: A Geochemical Study of the Carboniferous Audhild Volcanics, Northwestern Ellesemere Island, Arctic Canada: Initial Volcanism in the Sverdrup Basin

Date: 26 April 1989

Distribution License

DalSpace requires agreement to this non-exclusive distribution license before your item can appear on DalSpace.

NON-EXCLUSIVE DISTRIBUTION LICENSE

You (the author(s) or copyright owner) grant to Dalhousie University the non-exclusive right to reproduce and distribute your submission worldwide in any medium.

You agree that Dalhousie University may, without changing the content, reformat the submission for the purpose of preservation.

You also agree that Dalhousie University may keep more than one copy of this submission for purposes of security, back-up and preservation.

You agree that the submission is your original work, and that you have the right to grant the rights contained in this license. You also agree that your submission does not, to the best of your knowledge, infringe upon anyone's copyright.

If the submission contains material for which you do not hold copyright, you agree that you have obtained the unrestricted permission of the copyright owner to grant Dalhousie University the rights required by this license, and that such third-party owned material is clearly identified and acknowledged within the text or content of the submission.

If the submission is based upon work that has been sponsored or supported by an agency or organization other than Dalhousie University, you assert that you have fulfilled any right of review or other obligations required by such contract or agreement.

Dalhousie University will clearly identify your name(s) as the author(s) or owner(s) of the submission, and will not make any alteration to the content of the files that you have submitted.

If you have questions regarding this license please contact the repository manager at dalspace@dal.ca.

Grant the distribution license by signing and dating below.

_____ _____

Name of signatory Date

TABLE OF CONTENTS

ABSTRACT

Spilitized basalt flows constitute the largest portion of the Late Carboniferous Audhild Formation exposed on Kleybolte Peninsula, northwestern Ellesmere Island. The flows were erupted subaerially and are commonly separated by weathering horizons (paleosols), clastic sediments, and volcaniclastic or pyroclastic units. Stable trace element ratios show within-plate alkali affinities for the basalts, and regional stratigraphy indicates that Carboniferous volcanic activity was related to the early rift stage that led to development of the Sverdrup Basin. There is no geochemical evidence for fractional crystallization within the basalt suite. The volcanic rocks of the Audhild Formation probably represent primary magma derived by ~10% partial melting of a fertile mantle source. A series of basaltic dykes intruding the Audhild volcanic and sedimentary sequence shows no evidence of a genetic link to the flows, and is probably related to later Cretaceous magmatism.

ACKNOWLEDGEMENTS

First of all, I wish to thank my supervisor, Dr. Gunter Muecke, who not only guided me through this project, but also introduced me to geology and geochemistry, and developed my interest in these subjects over the past five years.

During the course of this thesis, I received helpful advice and valuable technical assistance from many people, but especially from Doug Merrett and Barry Cameron.

Robbie Hicks deserves special thanks both for the time and effort that she gave and for just being Robbie.

1. INTRODUCTION

1.1 Background

The Sverdrup Basin, with an area of about 300,000 square kilometres in the northernmost part of the Canadian Arctic Archipelago (figure 1), contains a nearly complete sequence of Early Carboniferous to Early Tertiary marine and nonmarine sediments and volcanics. This basin fill reaches a maximum thickness of 13,000 m in the central portion of the basin (Balkwill, 1978; Stephenson et al., 1987). Deposition was initiated by continental rifting and subsidence in the Carboniferous Period, and was terminated by uplift during the Eurekan Orogeny (mostly Tertiary) and by the opening of the adjacent Canada Basin (post - Jurassic).

The stratigraphy of the Sverdrup Basin has been mainly determined by reconnaissance and regional scale mapping by expeditions of the Geological Survey of Canada since circa 1950. This work has been substantially augmented by information from exploratory hydrocarbon wells. The Sverdrup Basin was actively explored for oil and natural gas in the 1960s and 1970s and as a sedimentary sequence, the rocks of the Sverdrup Basin are a potentially large reservoir of oil and gas. They contain numerous hydrocarbon showings, but remain a frontier province for exploration. As an igneous province, the Sverdrup Basin remains largely unknown and unexplored outside of current and very recent work. Sedimentary basins developed within areas of continental crust by rifting and thinning of the lithosphere can have a history

of magmatism as well as of subsidence and sedimentary infilling. Whether continental rifting is initiated by a rising mantle plume or if the upwelling of asthenospheric material is the passive result of lateral extension of the lithosphere, partial melting of the upper mantle may introduce a significant igneous component into the basin. The volume and composition of magma generated may be used to test the applicability of specific models to basin development. Igneous rocks within a sedimentary sequence are valuable indicators of the tectonic conditions that produced the basin.

The most voluminous igneous rocks in the Sverdrup Basin are Cretaceous flows, dykes, and sills (Williamson, 1988). Basaltic rocks related to the early rifting stage of the basin occur principally in the Carboniferous Audhild Formation and Permian Esayoo Formation (Thorsteinsson, 1974; Cameron, in prep.), but also as local volcanic units at Clements Markham Inlet on northernmost Ellesmere Island and within the Carboniferous marine clastics and carbonates of the Borup Fiord Formation on Axel Heiberg Island (Trettin, 1987; 1988). Figure 2 provides an illustration of the stratigraphic positions of these volcanic episodes. The subject of this study is the largely volcanic Audhild Formation, exposed on Kleybolte Peninsula near the northwest extremity of Ellesmere Island (figure 1, figure 3). The Audhild Formation is dated by its stratigraphic position between fossiliferous formations (Thorsteinsson, 1974), and is determined to be late Namurian or early Bashkirian (333 Ma - 305 Ma) (Geological Society of America, 1983). The type section, near the study location on Kleybolte

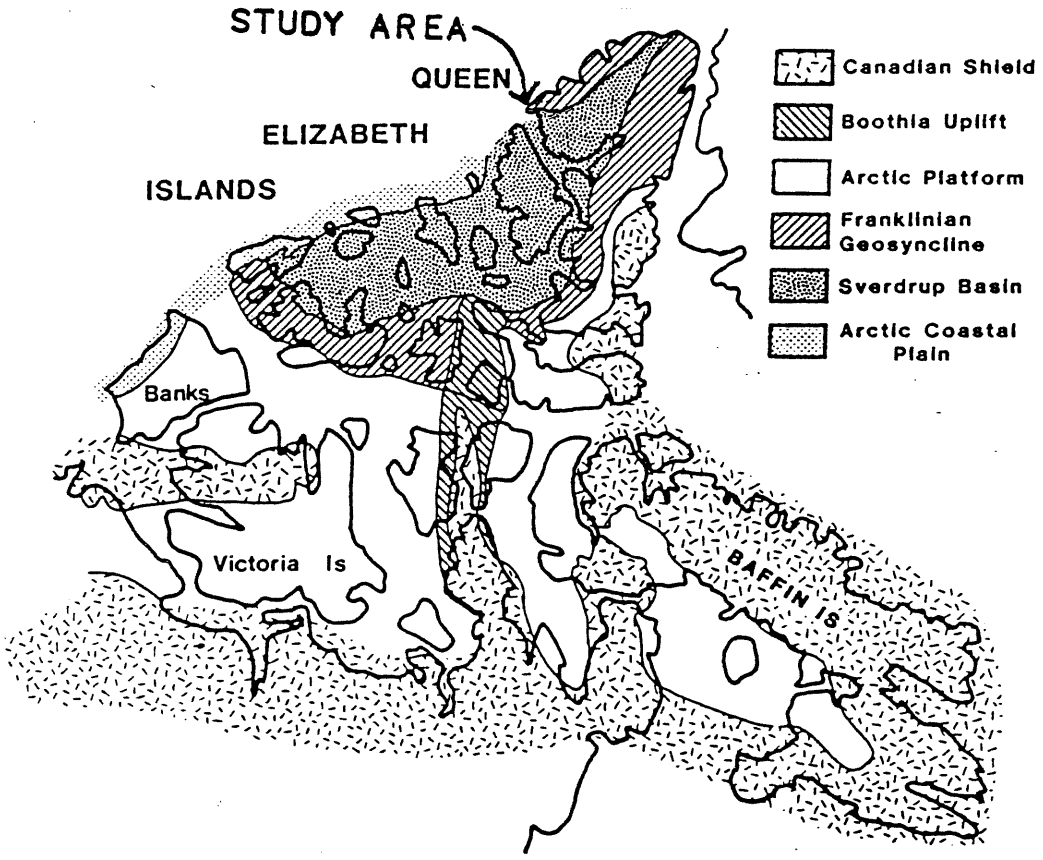

Figure 1. Geological setting of the Sverdrup Basin and location of study area.
Modified from Stephenson et al.,1987

Peninsula (figure 3), is described by Thorsteinsson (1974) as being made up of dark basalt and spilite, with subordinate pyroclastic sediments. Together with the volcanics of the Borup Fiord Formation (Trettin, 1987; 1988) and at Clements Markham, the Audhild Formation has particular importance in being the oldest known record of volcanism in the Sverdrup Basin (figure 2). These rocks record the initial rifting event that produced the Sverdrup Basin.

Basaltic flow units of the Audhild Formation in the study area have undergone extensive hydrous alteration and metamorphism to the zeolite or lower greenschist facies. As a consequence of this spilitization, the rocks retain little of their original igneous mineralogy, and may have experienced substantial chemical change.

1.2 Research Objectives

This thesis includes investigations of the mineralogy, petrology, and geochemistry of the Audhild flows and volcaniclastics, and of the basaltic dykes hosted by them. The immediate aim of this study is to determine the original composition of the altered and metamorphosed volcanics. Methods of discrimination between different magma types (e.g. alkali basalt, tholeiite, MORB) require a demonstration of the immobility of certain critical elements during the pervasive and at least moderately intense alteration observed in samples from the study area. More specifically, the objectives of this study include:

1. A description of the metamorphic mineral assemblage of the basalts and volcaniclastics in the Audhild

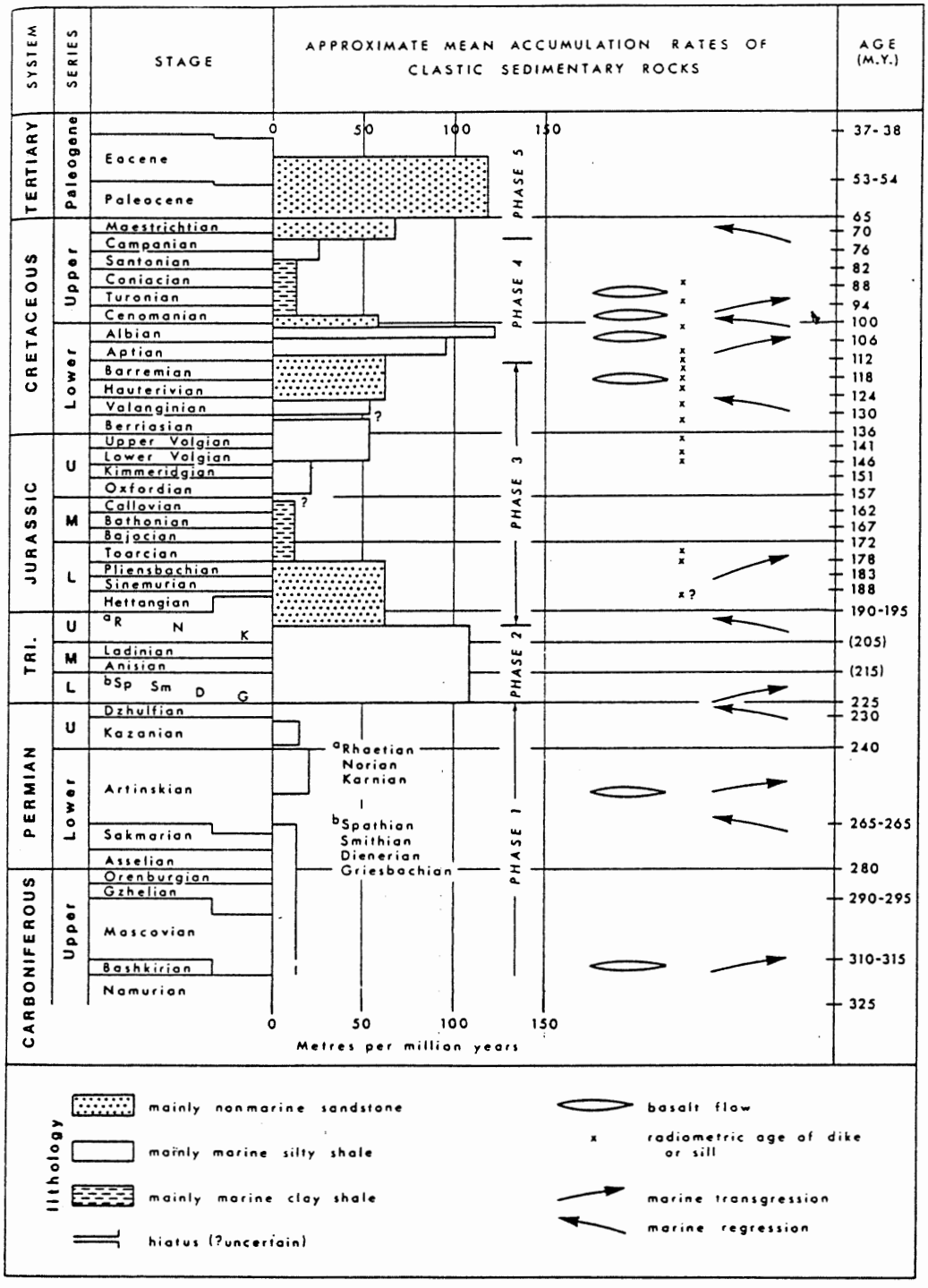

Figure 2. Diagrammatic History of Sverdrup Basin, showing stratigraphic position of Audhild Basalts. From Balkwill, 1978

Formation.

2. A test of whether any major or trace elements and the rare earth elements have remained immobile during alteration, and determination of the petrologic and petrogenetic implications of these stable element levels.
3. Analysis of intact igneous minerals to determine magmatic affinities of the original rocks.
4. Comparison of the chemistry of the basalts with that of the (as yet) undated intrusives to determine whether these two spatially associated occurrences of igneous rocks are likely to be part of the same magmatic cycle.
5. A comparison of the chemistry of the Audhild Formation with that of later volcanic episodes in the Sverdrup Basin.
6. Discussing the tectonic and geodynamic implications of the rock compositions e.g. degree of crustal thinning required to produce melting and eruption; degree of partial melting required to generate melts of the observed composition; mantle conditions (temperature, composition) beneath the incipient Sverdrup Basin.

2. GEOLOGIC SETTING

2.1 Regional Geology

The geology of the Canadian High Arctic can be divided into a small number of domains, corresponding to deformational and depositional stages. A series of geological provinces (figure 1) with progressively younger ages extends northward from the Precambrian cratonic interior to the Cenozoic continental margin of the Arctic Ocean. Most of eastern portions of the Arctic Archipelago are underlain by Churchill Province rocks of the Canadian Shield. These granitic and metamorphic rocks yield isotopic ages of about 1.7 Ga (Balkwill, 1978), corresponding to the Archean to Early Proterozoic Hudsonian Orogeny. Structural trends within these gneissic rocks are dominantly NE-SW to N-S and are cut by later structures of the north-trending Boothia uplift.

Proterozoic and Lower Paleozoic rocks of the Arctic Platform and Franklinian Geosyncline were deposited on the crystalline Hudsonian basement. These are mostly carbonates and shallow marine or nonmarine clastics. Franklinian strata were deposited on a cratonic shelf to the southeast and in a deeper water basin to the northwest (Trettin, 1973). The Pearya terrane (included as part of the Franklinian Geosyncline in figure 1) of northernmost Ellesmere Island is interpreted as a composite terrane accreted to the North American continent in late Silurian time. During the Middle Devonian to Early Carboniferous Ellesmerian Orogeny, these rocks were deformed and metamorphosed. Deformation and deposition were, in part, contemporaneous with clastic sediments being shed

into the Franklinian Basin from the orogenic front advancing to the southeast. The northeast striking folds and thrusts of the Ellesmerian Orogen parallel pre-existing tectonic structures and Franklinian depositional trends. Further Paleozoic tectonic activity in the Canadian Arctic includes continued intermittent uplift of the Boothia area that affected Precambrian basement as well as strata of the Arctic Platform and Franklinian Basin.

2.2 Sverdrup Basin

During the Early or Middle Mississippian, the Sverdrup Basin began to develop within the continental crust of the uplifted and eroded Franklinian mobile belt. The SW-NE axis of the basin parallels the structural trends of both the Franklinian belt and the older shield rocks. Present exposures of Sverdrup Basin strata coincide nearly to the areal extent of the Ellesmerian Orogen. Relative ages of the orogenic activity and earliest sedimentation show that rifting and extension closely followed the compressional stage. Upper Paleozoic rocks of the Sverdrup Basin include terrigenous clastics, mafic volcanics (erupted during two episodes, Late Carboniferous and Early Permian), and large quantities of carbonates and evaporites suggestive of restricted marine conditions. In contrast, the Mesozoic basin fill contains no evaporites and very little carbonate material (Balkwill, 1978). The oldest known lithological units of the Sverdrup Basin are Lower Carboniferous (Visean) clastics exposed on the basin rim in northern Axel Heiberg Island and northwestern Ellesmere Island, and near the basin margin on northernmost Devon Island (Thorsteinsson,

1974). Other Upper Paleozoic rocks occur along portions of the basin margin. The present observed limit of sedimentary rocks seems to coincide with the original areal extent of the Sverdrup Basin (Balkwill et al., 1983). Outcrops in the central part of the basin are of much younger age. In its overall geographic position, the Sverdrup Basin spans the boundary between continent and ocean. Its Mesozoic tectonic and sedimentary history overlaps with that of the adjacent Canada Basin (Arctic Ocean).

Seismic refraction data (citations in Stephenson et al., 1987) suggest that the pre-rift basement under the Sverdrup Basin is substantially thinned. The degree of thinning was greatest in that part of the basin that now contains the thickest accumulation of sediments. In the axial or central portion the crustal thickness was reduced by a factor of 2 of more (Stephenson et al., 1987). Near the margins, thinning, subsidence, and sedimentation were considerably less. Current theory on the genesis and evolution of rift basins stems from the pioneering work of McKenzie (1978). In either a simple conceptual model or a detailed mathematical formulation of basin development, lateral thinning of the lithosphere by shearing stresses is seen to result in subsidence of the surface and upwelling of asthenospheric material at depth. These two aspects occur in order to re-establish a condition approximating local isostasy. This early stage of subsidence is nearly contemporaneous with the process of rifting and crustal thinning. If stretching and upwelling are of sufficient magnitudes, decompression of the upwelled mantle material will induce partial melting, giving rise to magmatic activity (volcanic,

intrusive, or both) in the overlying sedimentary basin. As hot mantle material cools to re-establish an equilibrium geothermal gradient, and as sediment loading depresses the crust, there is a long (typically on the order of 100 Ma) phase of thermal subsidence due to thermal contraction. Stephenson et al. (1987) provide a detailed numerical model for the Permian to Early Cretaceous history of thermal subsidence in the Sverdrup Basin. In this model, a single episode of rifting in the Carboniferous and Permian is invoked to initiate the passive post-rift subsidence which continued until the onset of renewed extension during Cretaceous time. The Carboniferous and Permian volcanic sequences are the igneous products of this rifting phase.

2.3 Audhild Formation

Exposures of Carboniferous volcanic rocks related to development of the Sverdrup Basin are confined to the northwestern rim of the basin. This Sverdrup Rim is a complex feature which was tectonically active at many stages of basin development. Northwest provenance of some clastic units and localized unconformities near the basin margin suggest that the region was a positive topographic element for some time, but was also the locus of deposition and rift-initiated volcanism in both the Paleozoic and Mesozoic. Sediment transport into the basin from a northwestern source characterizes certain Middle Pennsylvanian, Triassic, and Jurassic units (Trettin, 1973), and some Permian sediments as well (Balkwill, 1978). This contribution is relatively minor, however, and Carboniferous and Permian sediments along the northwest basin

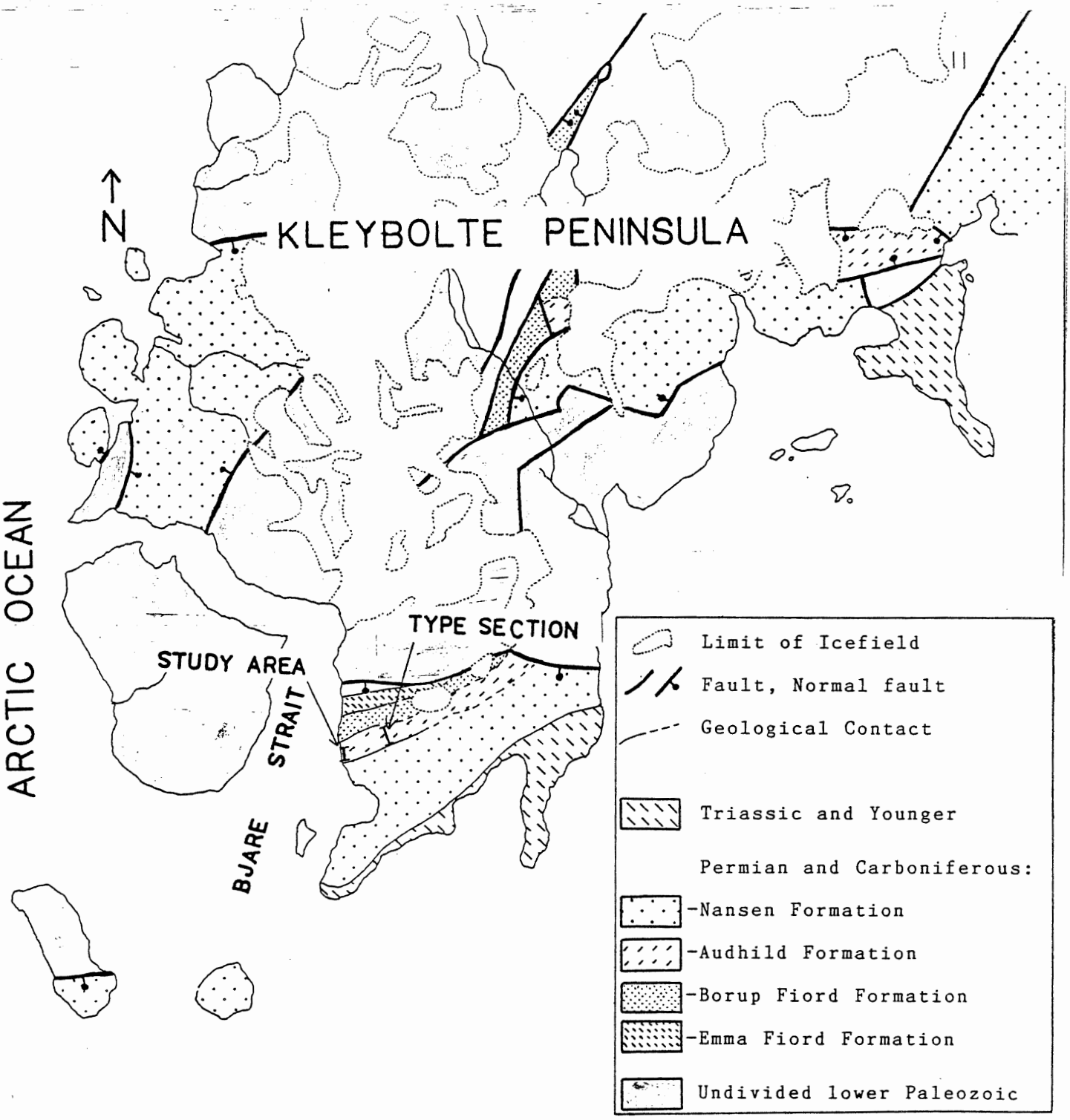

Figure 3. Geological map of Kleybolte Peninsula, Ellesmere Island, showing location of study area and of type section of Audhild Formation. Geology after Thorsteinsson and Tozer, 1970. Scale 1:150,000

margin generally contain less clastic material than those in the south or east. Unconformities of limited lateral extent can be considered as the result of relative uplift of fault blocks during rifting. The Sverdrup Rim has been greatly modified by tectonic activity related to the Mesozoic rift phase and to the Cenozoic development of the Canada Basin.

The Audhild Formation crops out over an area of about 10 km^2 in several fault blocks on Kleybolte Peninsula, Ellesmere Island (see figure 3 and Thorsteinsson and Trettin, 1970). The type section is located near the western coast of the peninsula (Thorsteinsson, 1974) and is described as being dominantly basalt with minor sediments. The Audhild Formation lies conformably upon the early Namurian Borup Fiord Formation, and is followed in succession by the Nansen Formation of Bashkirian and younger age. The Audhild Formation is laterally discontinuous; at other localities the Borup Fiord Formation is overlain directly by the Nansen (figure 9 of Thorsteinsson, 1974). Stratigraphically, the base of the Audhild is located some 700 m above the unconformity between Lower Paleozoic rocks and the Sverdrup Basin sequence.

3. ROCK UNITS AND DESCRIPTIONS

3.1 Stratigraphy

The exposed portion of the Audhild Formation along the west coast of Kleybolte Peninsula (see figure 3) was measured and sampled by Gunter Muecke and Doug Merrett during the 1987 field season. The section (figure 4 and plate 1) includes 6 m of clastic sediments with some volcanic contribution, 29 m of pyroclastic and volcaniclastic material, and 15 basaltic flows with an aggregate thickness of 74 m. Including two short covered intervals, a total of 114 m of stratigraphic section was measured, described, and sampled. This is the most complete section of the Audhild Formation that is amenable to sampling of in situ volcanic rocks. The immediate area is characterized by rubbly slopes and the less competent stratigraphic units are often not exposed. Localized shearing and tectonic disruption are also evident within the section. Thorsteinsson (1974) recorded a total thickness of more than 400 m for the Audhild Formation, but the type section, located several kilometers inland from the section measured in 1987, (indicated in figure 3) includes a considerable stratigraphic thickness with no outcrop.

A sheared green and maroon shale at the base of the studied section is probably reworked (epiclastic) material, if it has a volcanic component. This is overlain by a heterogeneous pyroclastic unit consisting of basalt fragments, pumice, and ash in multiple graded beds. Individual beds are on the order of 10 cm thick. The upper portion of this unit includes lensoidal

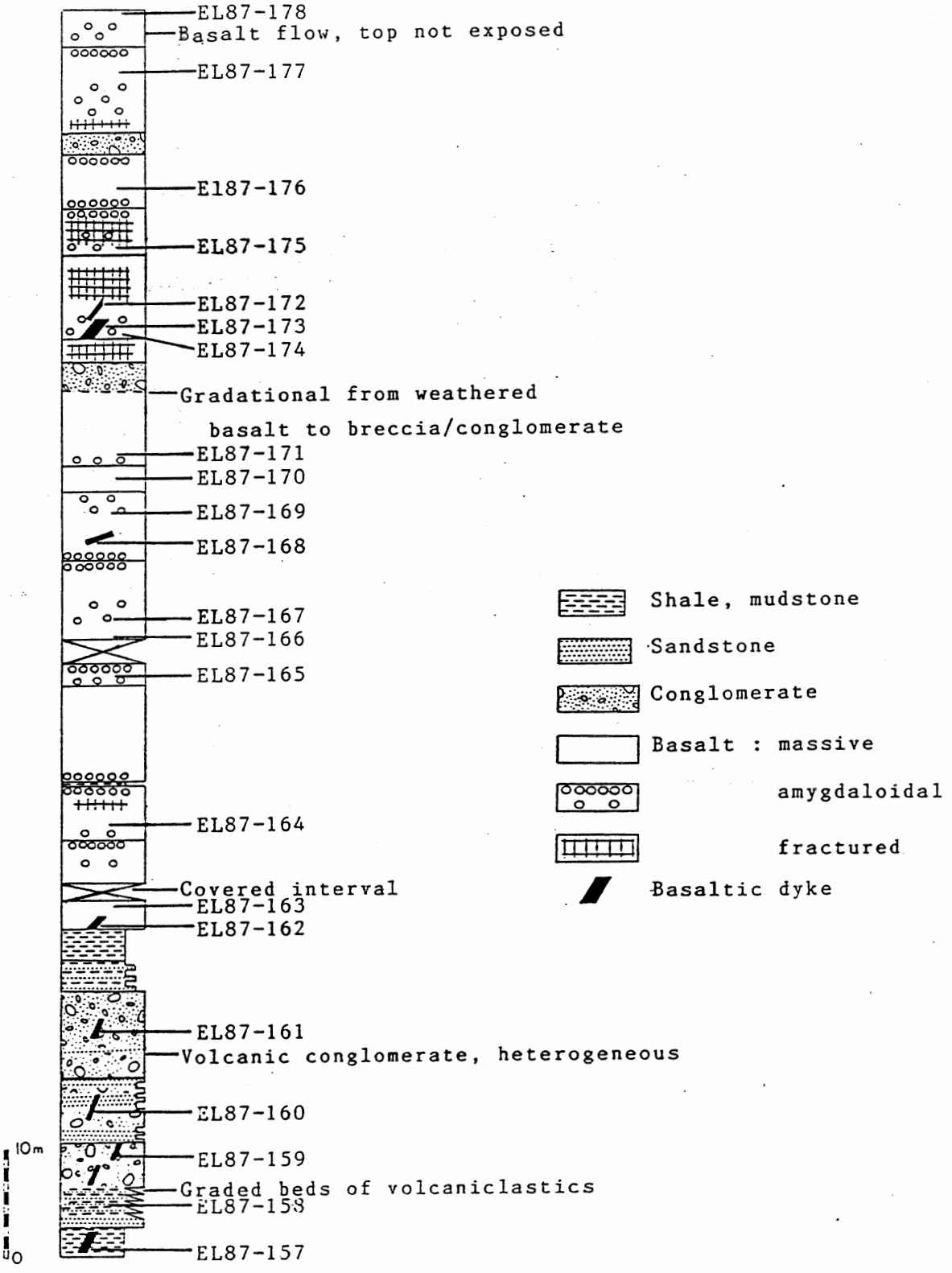

Figure 4. Stratigraphic Section, Coastal Exposure of Auhild Formation on Kleybolte Peninsula.

lapilli or bombs of basaltic composition. The flattened pumice and basaltic fragments suggest that the material was laid down while hot, and the unit is a possible pyroclastic fall deposit. A further sequence of interbedded pumice, fragmental basalt and probable ash material extends to 16 m. The fragments and pumice are flattened in the bedding plane, as in the underlying unit, although it contains rare quartz pebbles as well as volcanic materials (plate 2).

The segment from 16 m to 29 m includes poorly sorted subrounded basalt fragments, pumice, and quartz pebbles (plate 3). Channeling indicates that the basal part of this unit may be transported material, but a pyroclastic surge or flow is unlikely in view of the clast lithology (rounded fragments, pebbles) and lack of welding. This passes upward into maroon and green crossbedded sandstones, siltstones, and laminated mudstones that apparently are reworked volcaniclastic or non-volcanic material. The non-volcanic contribution to sedimentation suggests reworking of a largely (but not exclusively) volcanic terrain. A nearly continuous fining upward sequence is present in the entire segment, with waning evidence of volcanic influence. The siltstones at the top of this sequence are baked and bleached at the contact with an overlying series of basalt flows.

Nine basalt flows occur between 29 m and 78 m in the stratigraphic section. These flow units are all amygdaloidal in part. Some have amygdales at the base, but are massive in their central portion, suggesting that the lavas were erupted onto wet ground and incorporated volatiles from underlying sediments (plate

4) or interflow weathering horizons (paleosols). Where exposed, flow tops are all observed to be amygdaloidal to highly scoriaceous (plate 5). The uppermost flow of this series grades into a volcaniclastic breccia containing angular scoriaceous basalt fragments up to 20 cm supported in a matrix of sand or mud-size material. Based on texture and clast, this deposit is interpreted as the product of a volcanigenic mudflow or lahar.

The basal unit of a second series of basalts is a calcite-cemented breccia apparently produced by the fracturing of a basalt flow (tectonic disruption?, shear of a brittle layer?). In the three overlying flows, the pattern of amygdaloidal flow bases and tops is generally continued.

A two metre thick matrix-supported volcaniclastic conglomerate (plate 6) occurs 10 m from the top of the measured section. This probable mudflow deposit is similar to the breccia at 80 m, with scoriaceous basalt fragments in a sandy or silty matrix.

Two amygdaloidal basalt flows comprise the uppermost portion of the section. The top of the higher flow is covered, and there are no further bedrock exposures at the study area.

Pyroclastic deposits suggest that volcanic products were erupted with some violence, but there is insufficient exposure and stratigraphic control to indicate proximity of vents or volcanoes. The Kleybolte Peninsula section displays a progression from dominantly pyroclastic activity to relatively quiescent basaltic vulcanism, but it is not clear whether this pattern is retained throughout the whole of the Audhild Formation.

The basaltic flow units are commonly separated by weathering

layers or sediment, indicating that they are unlikely to have been erupted in rapid sucession, although the degree and likelihood of weathering and clastic deposition is highly dependent upon climate and tectonic environment. The amygdaloidal nature of the flow bases and tops indicates that the lavas were rich in volatiles, either when originally extruded or by incorporation of groundwater before solidification. The spilitization that characterizes the Audhild basalts suggests an influx of carbon dioxide and water. This addition of volatiles is confirmed by the chemical analyses reported in table 3; loss on ignition for the least altered basalt is the lowest of 14 analyses from flows. The alteration is not uniform in style or degree, and is more likely to have been an early post - eruptive process than a regional metamorphic event. No metamorphism is evident in carbonate and pelitic sediments above and below the Audhild Formation.

Eight basaltic dykes intrude the stratigraphic section. These intrusives range from 40 to 150 cm in width and exhibit a variety of textures and mineralogical compositions. Some of these bodies may have been feeder dykes to volcanic deposits within the Audhild Formation, or they may be the products of a much later stage of magmatism.

Continental-type redbeds of sandstone and conglomerate, with minor marine sediments dominate the underlying Borup Fiord Formation. The Audhild Formation, as exposed on Kleybolte Peninsula is apparently terrestrial. There is no evidence of pillow structure in the flow units and weathered zones or sediment horizons are commonly developed between flows. The overlying

Nansen Formation is dominated by limestones and marine sediments (Thorsteinsson, 1974).

3.2 Petrography

Uncertain field relations and the extent of metamorphism make distinctions between intrusive and extrusive units difficult. Textural and mineralogical features observed in thin section confirm and clarify the intrusive versus extrusive divisions made in the field. On the basis of observations of thin sections and hand samples (Appendix A), 5 tentative divisions have been made:

1. Porphyritic Basalt Flows
2. Pyroclastics
3. Inequigranular to Porphyritic Intrusives
4. Inequigranular to Subophitic Intrusives
5. Highly Porphyritic Intrusive

The 13 rock units mapped as basalt flows are all sparsely to moderately porphyritic or glomerophyric (plate 7), with 2 to 15% by volume of plagioclase, pyroxene, and relict olivine phenocrysts. All samples of basalt flows contain calcite $\pm$ chlorite replacements of olivine (or some other ferromagnesian mineral - clinopyroxene?) (plate 8). Seven of the samples contain plagioclase as phenocrysts including one which also contains clinopyroxene. The presence or absence of clinopyroxene seems to be controlled by the degree of alteration (Cameron, in prep.), as the cpx-bearing unit is the least altered.

Basaltic flows commonly exhibit a variably developed pilotaxitic to trachytic texture in the groundmass (plate 9), with

some degree of alignment of plagioclase microliths. Larger scale features noted in the field produce textural variations within units. These features include the presence of scoriaceous flow tops, basaltic weathering horizons, and the vertical distribution of amygdales. Mineralogical and textural features might also be expected to vary with position in a specific flow.

One sample (EL 87-158 at 6m in section) was taken from a heterogeneous bedded sequence of pyroclastic material. Most pyroclastic and volcaniclastic units are severely weathered and are therefore poorly exposed and not readily sampled. In thin section (plate 10) a fragmental texture is evident, with pumice and subangular quartz indicating a mixture of volcanic and non-volcanic components. The fine grained nature and pervasive alteration (dominantly sericitic) of the groundmass makes individual constituents unidentifiable. Some rectangular outlines of sericitized plagioclase crystals are visible.

All intrusive rocks are distinctly less altered than the volcanic units. Their primary mineralogy and textures are more evident in thin section. Five intrusive rocks (EL 87-159, -162, -168, -172, -173) have been grouped together on the basis of their fine grained inequigranular to slightly porphyritic texture. These rocks are moderately altered with 10 to 20% chlorite and common fine grained alteration products. Plagioclase, occurring both as phenocrysts and in the groundmass, is moderately or extensively replaced by sericite. Primary opaque minerals (plate 11) are blocky or acicular (skeletal).

Samples EL 87-157 and EL 87-161 are slightly altered basaltic

dykes with a sub-ophitic texture of plagioclase (sericitized) and clinopyroxene (plate 12). Both dykes contain rare sericitized plagioclase phenocrysts. Opaque grains comprise 15% of the rocks and chlorite and fine grained alteration products are relatively minor constituents.

A single sample, EL 87-160, is composed of 35% subhedral or euhedral plagioclase phenocrysts up to 7 mm in a groundmass of purple-brown clinopyroxene, sericitized and chloritized plagioclase laths, granular opaque minerals,interstitial calcite, and calcite + chlorite aggregates (plate 13).

3.3 Mineralogy and Metamorphism

The evident disequilibrium textures may make use of the term "mineral assemblage" inappropriate, but the mineralogy of the altered basaltic rocks remains an indicator of their metamorphic grade. The dominant mineral in all basaltic samples is sericitized plagioclase, typically present as 1mm albite laths and less commonly as phenocrysts up to 6mm. Chlorite is present in all sampled flow units, and has several modes of occurrence. In the groundmass, chlorite is sometimes present as vague green patches but more commonly as discrete interstitial green or green-brown pleochroic grains. Chlorite is a common component in replacements of olivine phenocrysts. In samples EL 87-175 and EL-87-178, bright green chlorite occurs with calcite in amygdales. In EL 87-176, chlorite is present with calcite in a narrow veinlet.

Calcite is commonly observed in association with chlorite, secondary opaque minerals, and "iddingsite" as pseudomorphs after

olivine. It is also present as coarse grained cavity, vug, and vein fillings, and less commonly as a groundmass mineral.

Opaque minerals have several modes of occurrence. Primary opaques exist as blocky grains constituting 10 to 20% by volume of the rocks. The different morphologies (e.g. square cross-section, irregular) are indicative of the variety of minerals that are not distinguished optically. Skeletal crystals of opaque minerals occur in several intrusive rocks. Secondary opaque minerals are common along fractures and rims of relict olivine phenocrysts and as fine grained "dusty" material. In sample EL 87-175, a botryoidal opaque mineral is present as a secondary cavity filling phase (plate 14).

Quartz is found in four flows as a secondary mineral in amygdales. A single occurrence of quartz in the groundmass of a basalt flow is also considered to be of a secondary nature.

Zeolite minerals are present with calcite, quartz, and chlorite in amygdales in two samples. The minerals were not identified optically, but are characterized by radiating crystal habit and low birefringence.

The distribution of zeolites and quartz seems likely to have been controlled by the availability of cavities, which is in turn a function of volatile content of the lava, and may therefore vary with position in a flow unit. Permeability and the presence of fluids will influence the intensity of metasomatism or of chemical mobility within a rock unit. These are important factors in developing the secondary mineralogy as both original magma composition and post - depositional fluid circulation may

influence chemical and mineralogical changes. The secondary mineral "assemblage" calcite + chlorite ± zeolites ± silica indicates that the Audhild volcanic rocks have undergone burial metamorphism to lower greenschist grade. This grade and degree of alteration can be developed in mafic rocks in a near-surface or diagenetic environment (e.g. Best, 1982) and does not imply a regional attainment of the pressure and temperature conditions associated with greenschist facies metamorphism.

3.4 Mineral Chemistry

The chemistry of primary minerals that have not been destroyed by metamorphism and metasomatism can be used as an indicator of the magmatic character of altered basalts.

Electron microprobe analyses of clinopyroxenes were obtained for all pyroxene-bearing rock units. This includes all intrusives and the single basaltic flow in which pyroxene is preserved. A selection of plagioclase grains was also analyzed. The results are presented in appendix B.

Analyses of unaltered plagioclase grains (Table 1) support the identification of the extrusive rocks as basalts rather than andesites or trachybasalts.

Table 1

Plagioclase Composition

SAMPLE	An	Ab	Or	Comment
EL 87-157 (dyke)	62.0	37.8	0.2	Core
	45.2	53.5	1.3	Groundmass
	40.6	57.9	1.5	Rim
	67.2	32.7	0.1	Core
EL 87-160 (dyke)	75.1	24.6	0.3	Phenocryst
	74.5	24.8	0.6	Phenocryst
EL 87-176 (flow)	61.9	36.0	2.1	Near rim
	64.0	34.2	1.8	Core
	53.6	43.7	2.8	Intermediate rim-core
	61.6	36.3	2.1	Core

Three of the samples are distinguished by the presence of titanaugite (greater than 2 wt% TiO_2) (Deer et al., 1963), as illustrated in table 2.

Atomic proportions of Ca, Fe, and Mg show (figure 5) pyroxenes from all samples to be augitic or salitic in composition. In some intrusives (those with high TiO_2), calcium approaches 55 mole per cent of these ternary components. Pyroxenes in El 87-176 are clearly a phenocryst phase, but the crystals appear to have remained in equilibrium with the liquid portion of the magma, as no zonation of Ca, Mg, Fe, or TiO_2 content is evident.

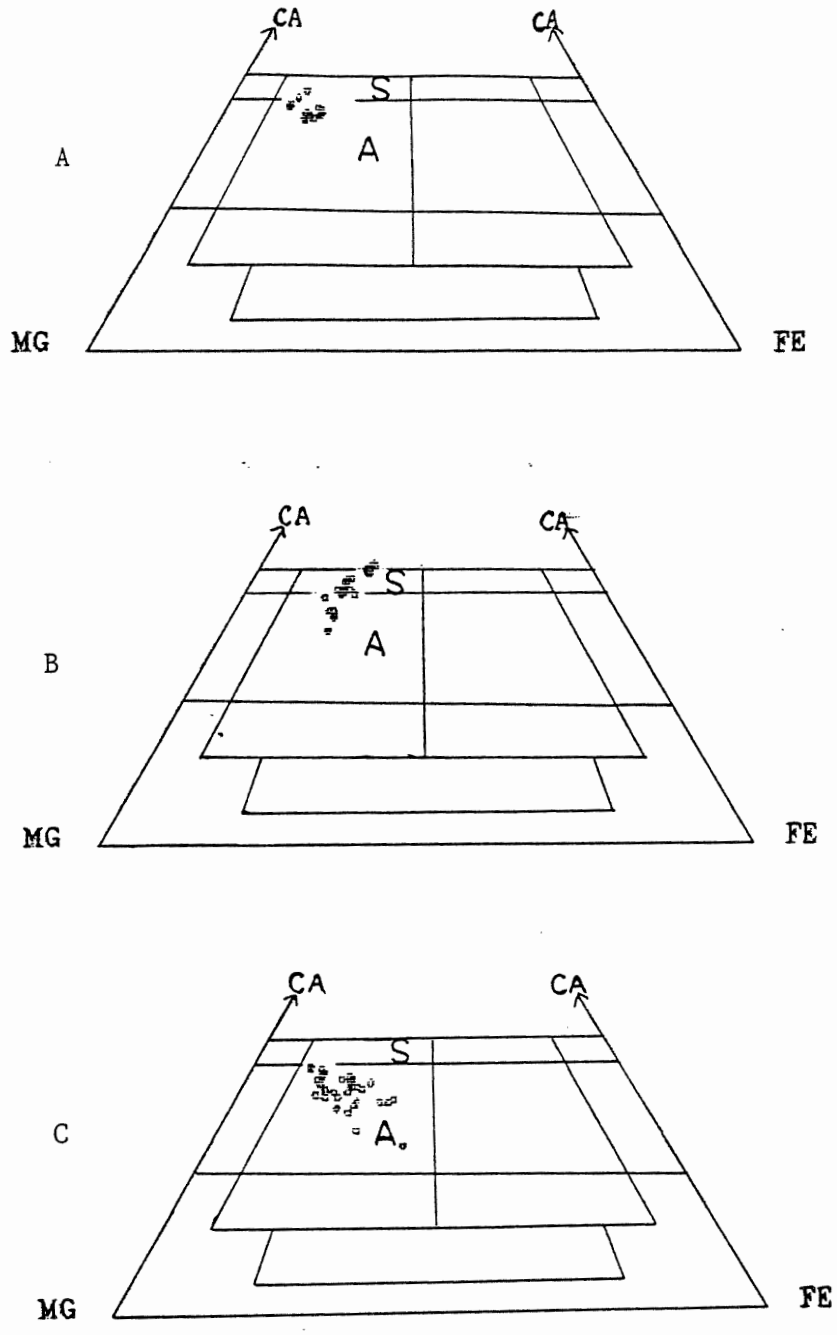

Figure 5. Clinopyroxene Compositions.
a) Clinopyroxene in Basalt (n=15).
b) Titanaugite in Intrusives (n=26).
c) Low-titanium Clinopyroxene in Intrusives (n=34).
Field S = Salite, Field A = Augite.

Table 2

Titanium Content of Clinopyroxenes

SAMPLE	MEAN WT% TiO_2	S.D.	N
EL 87-157	0.88	0.33	8
EL 87-159	2.72	0.35	8
EL 87-160	4.22	0.56	7
EL 87-161	0.68	0.32	12
EL 87-162	1.51	0.13	4
EL 87-168	1.46	0.32	8
EL 87-172	1.78	0.09	2
EL 87-173	2.00	0.65	11
EL 87-176	1.40	0.31	15

4.GEOCHEMISTRY

4.1 Methods

In order to further characterize the igneous rocks of the Audhild Formation, and to gain some insight into their igneous affinities and possible origins, 23 samples (including two duplicates) were prepared and submitted for X-ray fluorescence analysis of major and trace elements. Samples were prepared by removal of weathered surfaces from a circa 150 g portion of rock, followed by crushing and milling to -80 mesh and homogenization of the resultant powder. Analyses for loss on ignition, 10 major and minor element oxides, and 15 trace elements were performed by staff of the Atlantic Regional X-Ray Fluorescence Laboratory at Saint Mary's University, Halifax, Nova Scotia. Loss on ignition was determined as the mass lost after heating to 1050 C for 4 hours. It is assumed that this heating also converts ferrous iron to ferric, so that total iron is reported as Fe_2O_3. A subset of 10 samples was submitted to the Instrumental Neutron Activation Analysis Facility at Saint Mary's University for analysis of rare earth elements (REEs) and a further selection of trace elements. These 10 rocks were chosen to reflect the range of compositional types and degrees of alteration.

4.2 Results

The major and trace element contents are summarized in table 3. The full dataset is presented in Appendix C. An early observation, based on this data, is that the intrusive and

Table 3a
XRF and INAA Analysis of Major and Minor Element Oxides (wt %) and Trace Elements (ppm) - Basalt Flows
(14 analyses, 6 for INAA)

	Range	Mean	S.D.
SiO_2	46.21 - 55.11	51.04	2.47
TiO_2	1.92 - 2.71	2.81	0.20
Al_2O_3	13.32 - 16.30	14.62	0.90
Fe_2O_3	5.16 - 13.88	10.51	2.45
MnO	0.10 - 0.17	0.12	0.02
MgO	4.82 - 8.46	6.40	1.35
CaO	6.44 - 13.64	9.82	2.53
Na_2O	2.76 - 5.62	4.17	0.94
K_2O	0.31 - 2.80	1.50	0.82
P_2O_5	0.30 - 0.51	0.40	0.07
Total	100.34 -101.23	100.83	0.29
L.O.I	5.70 - 10.60	8.19	1.56
Ba	64 - 508	253	175.8
Rb	8 - 47	25	12.7
Sr	112 - 483	229	97.5
Y	18 - 25	22	2.4
Zr	134 - 287	199	32.4
Nb	23 - 53	40	8.8
Ga	16 - 21	18	1.5
Zn	40 - 159	74	28.8
Cu	13 - 34	24	14.8
Ni	178 - 358	226	60.3
V	181 - 266	213	26.1
Cr	316 - 555	391	65.9
Sc	20.1 - 24.3	21.8	1.4
Hf	4.48 - 5.53	5.00	0.39
Th	3.56 - 8.06	5.47	1.56
Ta	2.66 - 3.90	3.39	0.42
Co	29.5 - 51.3	37.4	8.8
La	23.4 - 36.8	30.5	4.6
Ce	49.7 - 74.5	62.2	8.4
Nd	24.3 - 31.3	28.3	2.6
Sm	5.32 - 6.94	5.92	0.58
Eu	1.47 - 2.12	1.82	0.21
Tb	0.73 - 0.81	0.77	0.04
Yb	1.67 - 1.99	1.84	0.14
Lu	0.25 - 0.33	0.28	0.03

Table 3b
XRF Analysis of Major and Minor Element Oxides (wt%)
and Trace Elements (ppm) - Volcaniclastic
(1 analysis)

SiO_2	53.30
TiO_2	3.26
Al_2O_3	20.22
Fe_2O_3	9.46
MnO	0.04
MgO	5.40
CaO	0.99
Na_2O	0.97
K_2O	6.16
P_2O_5	0.33
Total	100.14
L.O.I.	4.30
Ba	925
Rb	130
Sr	74
Y	23
Zr	302
Nb	63
Ga	23
Zn	32
Cu	0
Ni	250
V	318
Cr	309

Table 3c
XRF and INAA Analysis of Major and Minor Element Oxides (wt %)
and Trace Elements (ppm) - Intrusive Rocks
(8 analyses, 4 for INAA)

	Range	Mean	S.D.
SiO_2	46.61 - 50.33	49.01	1.25
TiO_2	1.80 - 3.94	2.98	0.89
Al_2O_3	13.26 - 22.04	14.83	2.95
Fe_2O_3	8.51 - 14.38	12.90	1.88
MnO	0.11 - 0.28	0.21	0.05
MgO	4.03 - 6.55	5.27	0.90
CaO	5.36 - 11.48	8.27	2.52
Na_2O	2.16 - 4.58	3.12	0.74
K_2O	0.54 - 3.76	2.18	1.44
P_2O_5	0.20 - 1.19	0.52	0.32
Total	98.50 -100.43	99.28	0.75
L.O.I.	0.50 - 4.40	2.33	1.42
Ba	91 - 1489	614	487.7
Rb	14 - 14	42	24.7
Sr	236 - 1182	546	375.6
Y	15 - 43	32	8.6
Zr	145 - 301	220	62.2
Nb	11 - 46	28	12.9
Ga	19 - 24	21	1.8
Zn	67 - 146	111	25.7
Cu	7 - 185	65	74.4
Ni	13 - 74	35	24.7
V	194 - 475	356	96.4
Cr	15 - 121	53	50.8
Sc	17.4 - 41.4	32.2	11.4
Hf	2.74 - 6.91	4.23	1.84
Th	1.10 - 5.31	2.47	1.96
Ta	0.98 - 2.28	1.57	0.67
Co	35.4 - 56.3	48.9	9.8
La	10.3 - 31.9	18.4	10.3
Ce	25.5 - 73.5	42.3	22.5
Nd	16.8 - 41.4	24.3	11.6
Sm	4.68 - 9.08	5.82	2.17
Eu	1.63 - 2.72	1.92	0.53
Tb	0.54 - 1.35	0.90	0.34
Yb	1.38 - 3.56	2.68	0.92
Lu	0.22 - 0.57	0.44	0.15

extrusive rocks are readily distinguishable on the basis of their chemical composition (e.g. figure 6). This confirms the separation based on field and petrographic observations noted in Chapter 3. The ranges of Cr and Ni values for the Permian episode of volcanism (Cameron, in prep.) are indicated for comparison. Higher values of both Cr and Ni for the Permian basalts overlap with lower levels from the Audhild volcanics. The generally lower degree of alteration that is visible in intrusive rocks is confirmed by the considerably smaller loss on ignition (volatile content). The single analysis for volcaniclastic material shows high levels of Al_2O_3, K_2O, and Rb relative to the basaltic rocks of the volcanic sequence. The elevated Al and alkali contents are consistent with the presence of a substantial clay component which could be developed from weathered volcanic material (glass) or may be transported from a non-volcanic source. CaO and Sr are strongly depleted in the volcaniclastic unit, suggesting that it contains highly leached material.

4.3 Trace Element Chemistry

4.3.1 Chemical Classification of Basalts

The metamorphism that is evident from mineralogical and textural changes may have had an effect on the bulk rock compositions as well. The mobility (and possible addition or loss) of SiO_2, MgO, Fe_2O_3 (and FeO), CaO, Na_2O, and K_2O is indicated by the presence of the secondary minerals quartz, chlorite, sericite, chlorite, zeolite, and opaque oxides. Elements that show clear evidence of post-magmatic mobility cannot be used to classify or

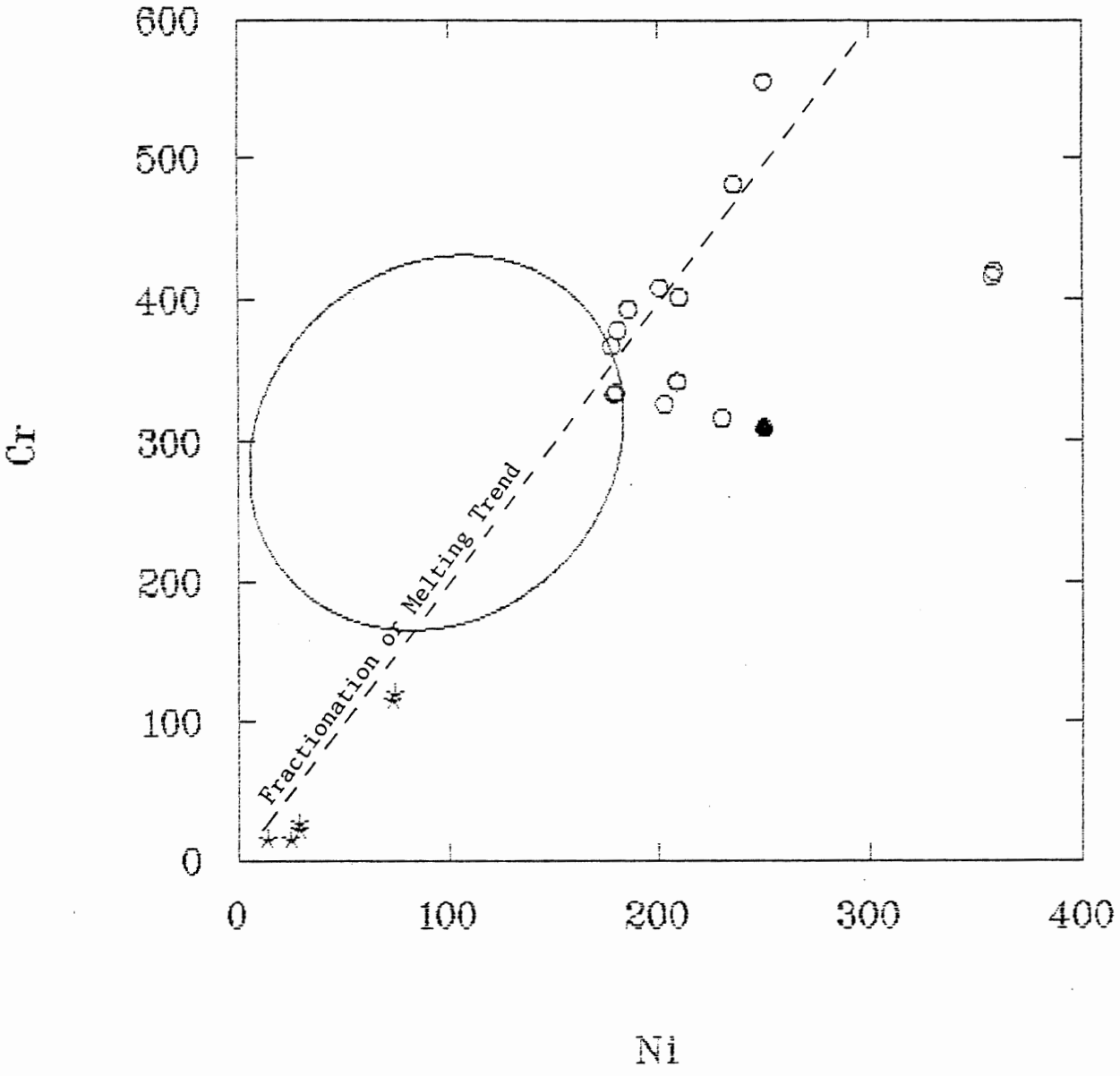

Figure 6. Chromium (ppm) vs Nickel (ppm). Extrusive (O = Basalt, ● = Volcaniclastic) and Intrusive (✶) Rocks from the Auhild Formation are clearly separated on this diagram. The large ellipse indicates the range in which 85% of the basalt flows of the Permian Esayoo Formation plot.

characterize the original igneous rocks. The nomenclature and classification of basaltic rocks (e.g. tholeiite versus alkali basalt) is based primarily on modal or normative mineralogy. Since mineralogy is dependent upon chemical composition, basalts can also be divided and named on the basis of chemistry. The ratio of silica to potassium plus sodium is indicative of basalt type (e.g. MacDonald and Katsura, 1964). The alkali-silica plot (figure 7) exhibits a considerable scatter that is interpreted as the result of alkali and/or silica mobility. In fresh cogenetic volcanic suites, both Na and K are expected to increase with SiO_2, producing linear trends. Mobility of alkali elements or silica (or both) in Audhild basalts has the result that this rock suite cannot be classified on the basis of these common (and commonly used) constituents. Intrusive and extrusive rocks are not separable on this diagram. Evidence for mobility of calcium is provided by a plot of CaO versus MgO (figure 8), which is expected to display either a linear trend or a tight cluster for an unaltered suite.

Trace and minor element concentrations and element ratios that can be demonstrated to be the result of igneous processes may be useful in classifying the metamorphosed basalts. High field strength ions (high charge/radius ratio) are not readily transported in aqueous fluids (Pearce and Norry, 1979), and may therefore be largely unaffected by low grade metamorphism. Ti, Y, Zr, Nb, P, and rare earth elements (REEs) are generally considered to have limited mobility, and have been demonstrated to be immobile in specific studies (e.g. Muecke, 1983). These elements are characteristic of rock types and have often been used to uncover

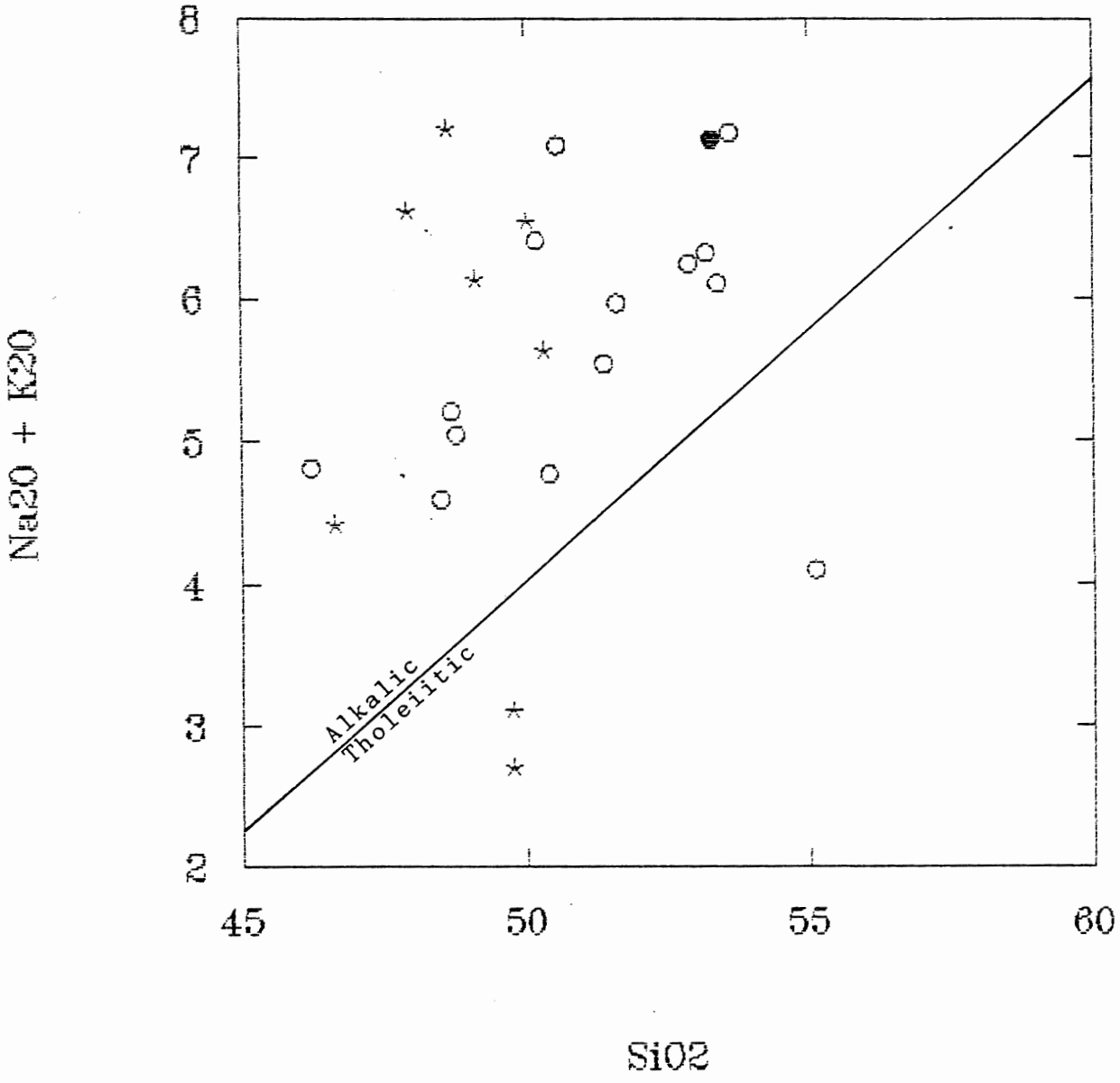

Figure 7. Alkali - Silica Plot Showing Division Between Tholeiitic and Alkalic Basalt (MacDonald and Katsura, 1964)
O = Basalt, ● = Volcaniclastic, ★ = Intrusive
Oxides in Wt.%.

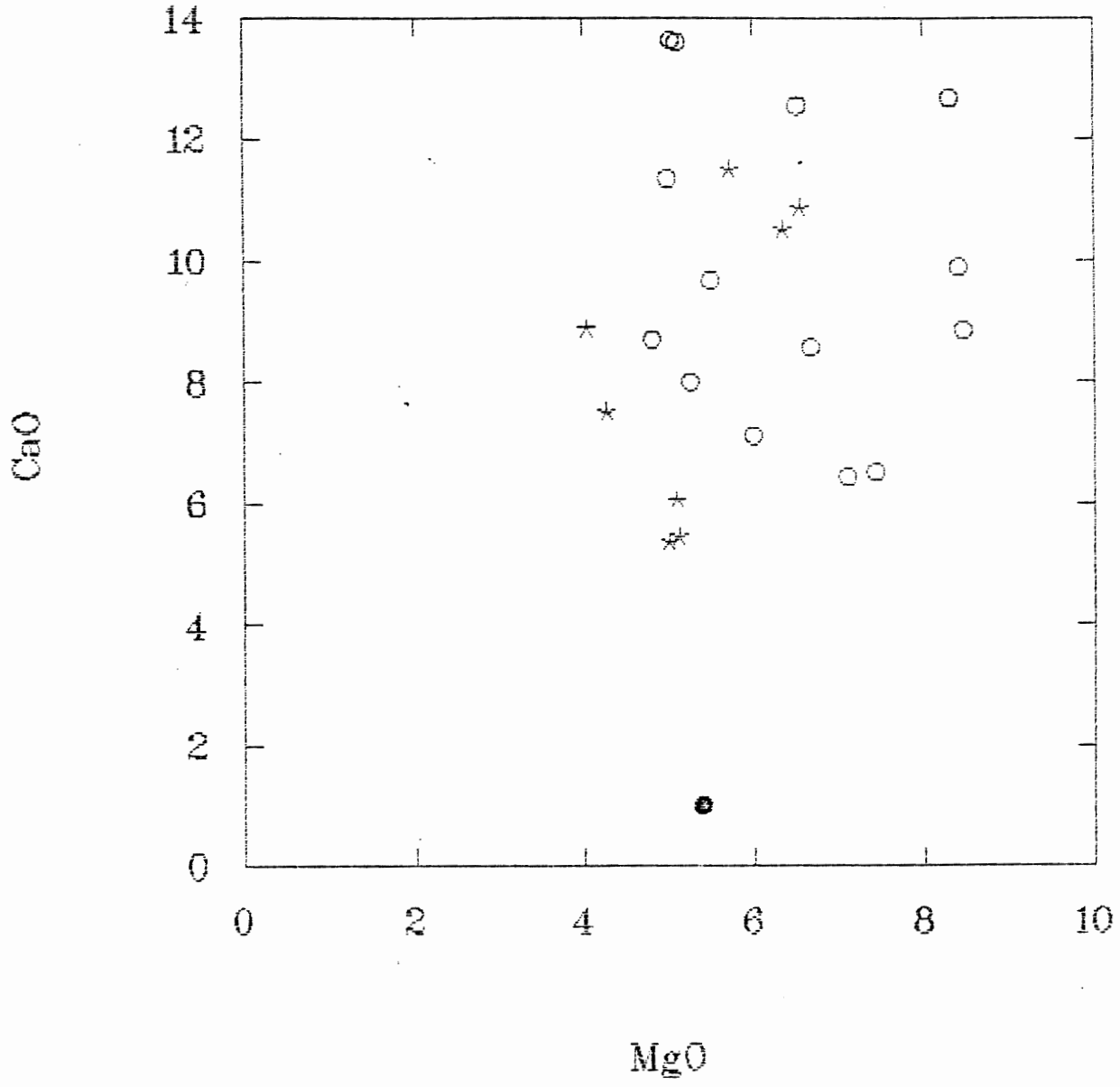

Figure 8. CaO (wt%) vs. MgO (wt%) Variation Diagram Showing No Igneous Trends.

○ = Basalt
● = Volcaniclastic
✶ = Intrusive

the original magmatic affinity and primary igneous character of altered volcanic rocks. Elements with large ionic size or high charge do not readily fit into the crystal lattices of silicate minerals, and are concentrated into the melt phase of a magma-solid equilibrium system. Concentrations of incompatible or hygromagmatophile elements will vary according to the degree of partial melting or crystal fractionation and should therefore show good correlations within cogenetic suites of erupted rocks. The absolute concentrations can vary significantly as a result of the magmatic processes of melt generation and differentiation; they may therefore be considerably different between portions of the same flow sequence or even within a single flow. The ratios should remain constant if the elements are behaving similarly. Absolute concentrations, however, may also be affected by dilution or concentration during bulk metasomatic addition or subtraction of other material. If the variations in these minor and trace elements are the result of igneous processes and they have not been mobilized during post-magmatic processes, they should retain correlations and may be useful in describing the rocks. For the volcanic units of the Audhild Formation, the retention of strong correlations is an indication that Y/Zr, Nb/Zr, TiO_2/Zr, and P_2O_5/Zr ratios have not been greatly modified by metamorphism and alteration (Table 4 and figure 9). Zr is useful as an index of fractionation because it behaves as an incompatible element since zircon, the principal Zr-bearing mineral, is a late phase in basalt crystallization (Deer et al, 1962). If the ratios are not constant, the trends do not lead to the origin. In such cases the

Table 4

Pearson Correlation Matrices

a: Extrusive Rocks, 14 Samples (6 for sumREE)

	Zr	Y	Nb	TiO_2	P_2O_5
Zr	1.000				
Y	0.719	1.000			
Nb	0.826	0.566	1.000		
TiO_2	0.216	0.022	0.311	1.000	
P_2O_5	0.820	0.504	0.869	0.562	1.000
sumREE	0.239	0.467	0.951	0.289	0.221

b: Intrusive Rocks, 8 Samples (4 for sumREE)

	Zr	Y	Nb	TiO_2	P_2O_5
Zr	1.000				
Y	0.737	1.000			
Nb	0.631	0.094	1.000		
TiO_2	0.793	0.718	0.575	1.000	
P_2O_5	0.762	0.290	0.887	0.505	1.000
sumREE	0.986	0.613	0.773	0.893	0.964

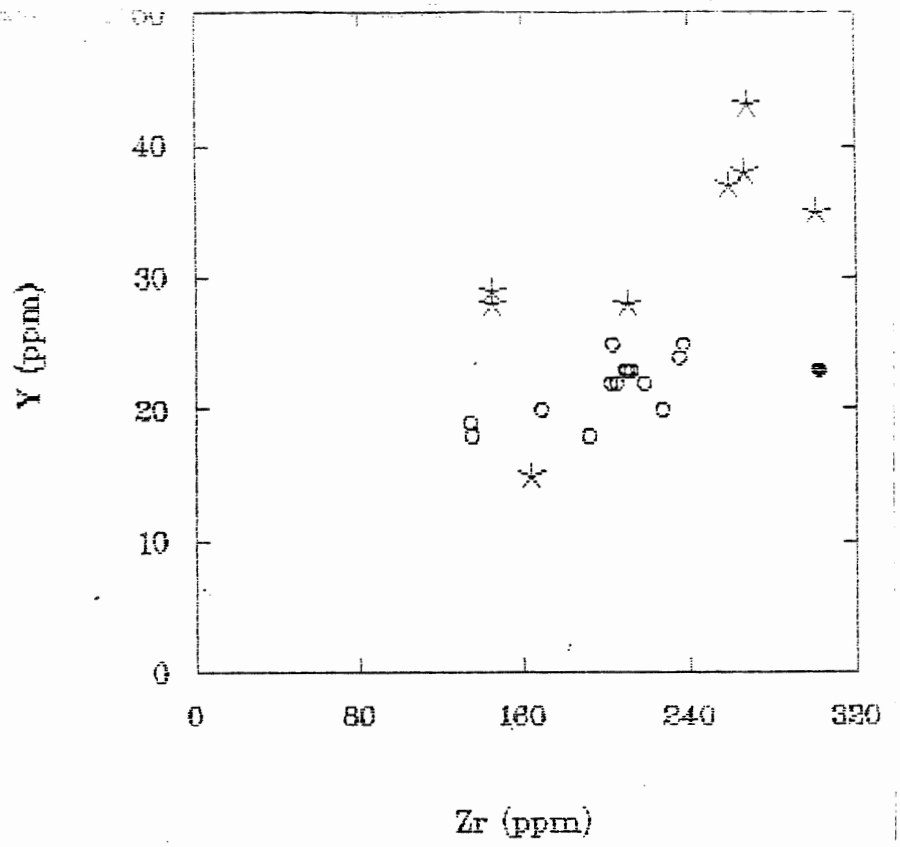

Figure 9a. Y (ppm) vs. Zr (ppm).

○ = Basalt, ● = Volcaniclastic, ★ = Intrusive

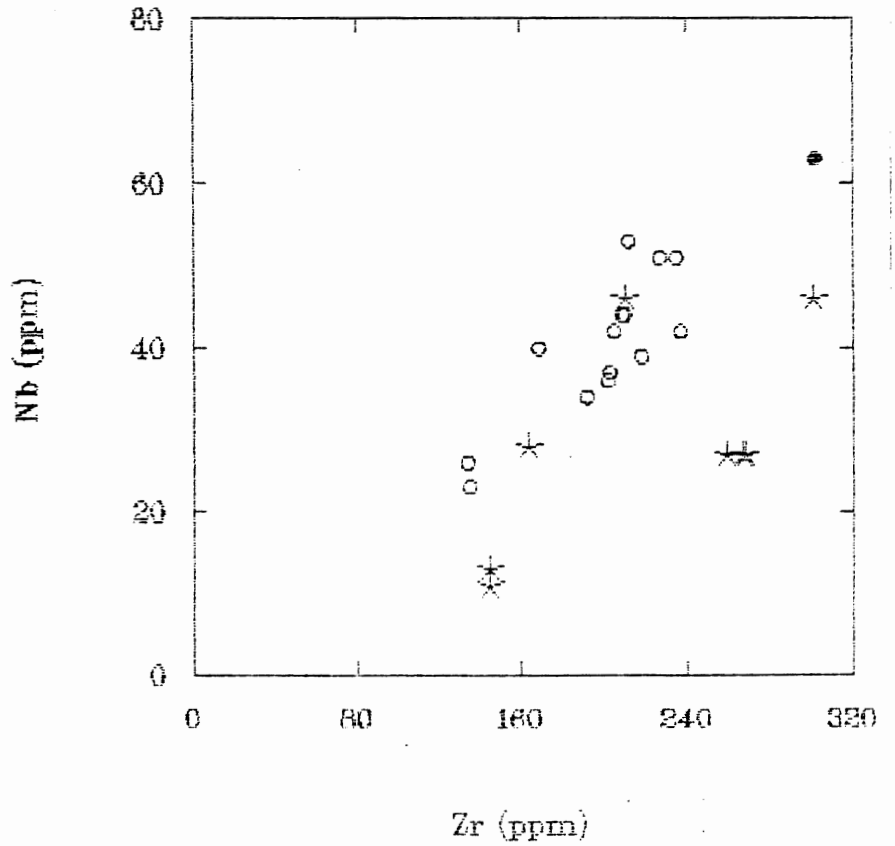

Figure 9b. Nb (ppm) vs. Zr (ppm).

○ = Basalt, ● = Volcaniclastic, ★ = Intrusive

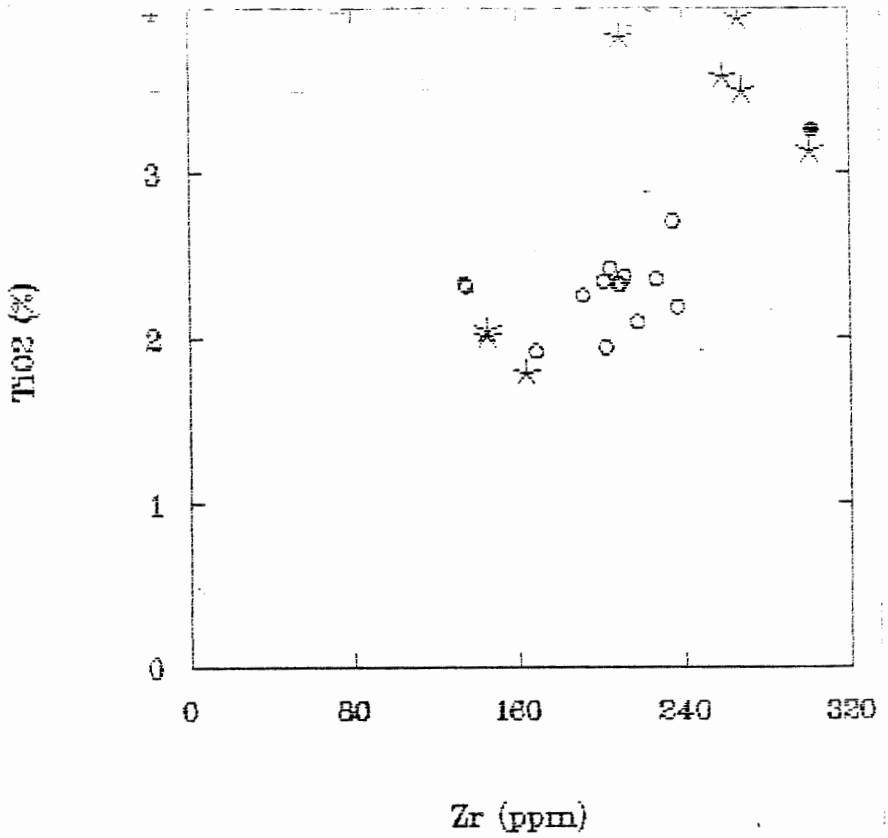

Figure 9c. TiO_2 (wt.%) vs. Zr (ppm).
○ = Basalt, ● = Volcaniclastic, ★ = Intrusive

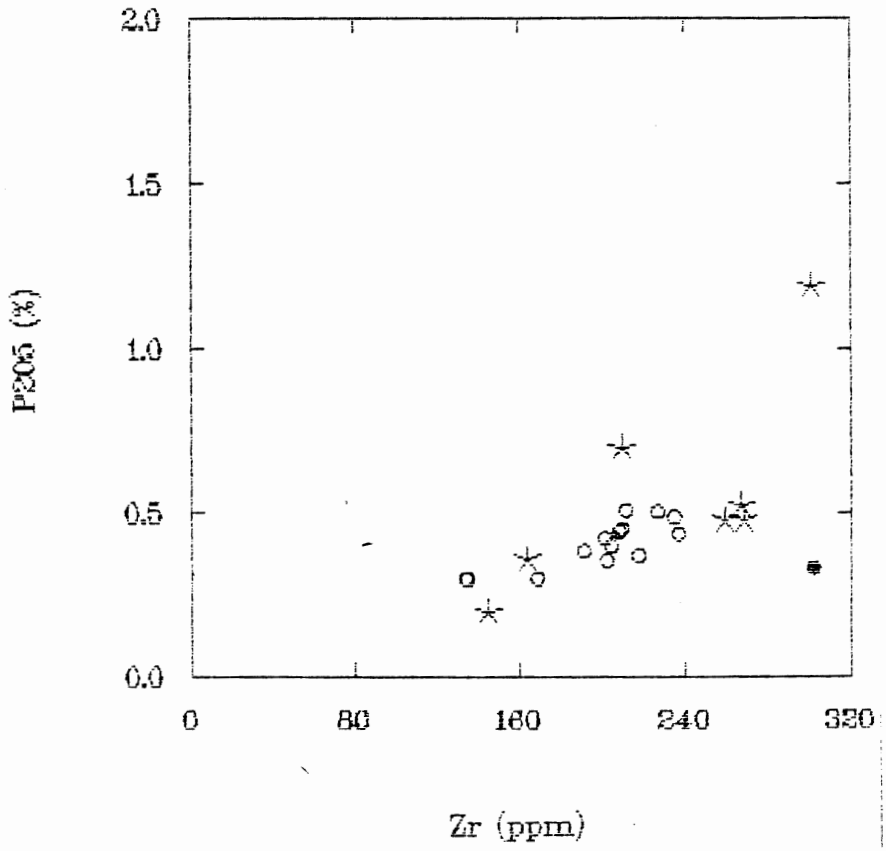

Figure 9d. P_2O_5 (wt.%) vs. Zr (ppm).
○ = Basalt, ● = Volcaniclastic, ★ = Intrusive

two elements are not behaving similarly because one has a lower crystal:melt distribution coefficient (defined as D = concentration in solid / concentration in coexisting liquid) or because one is preferentially enriched by some process of contamination. The intrusive rocks included in this study are not expected to display linear trends, even though they are less altered and less likely to have undergone element redistribution, because they do not necessarily have a common origin.

A classification of basalt types based on Zr/TiO_2 and Nb/Y ratios has been developed by Winchester and Floyd (1977). Audhild volcanic rocks plot in the alkali basalt field of this diagram (figure 10). Three intrusives (EL87-159, EL87-160, EL87-173) are also classed as alkali basalt, while the remainder are subalkaline.

Pearce and Cann (1973) proposed a division between alkalic and tholeiitic basalt types based on Nb/Y ratio. In an attempt to classify and separate intrusive from extrusive rocks of the Audhild Formation, P_2O_5 and TiO_2 have been plotted against Nb/Y (figure 11). Phosphorus and titanium are two minor constituents that vary considerably, but both are generally present at higher levels in the intrusives. Nb/Y is a measure of alkalinity, while the concentrations of incompatibles such as TiO_2 and $P2O_5$ can be considered as measures of differentiation. The data from extrusive rocks plot as an elongate cluster or subhorizontal trend. Absolute values and element ratios from intrusive rocks are widely spread. The three alkalic intrusives have Nb > Y ; EL 87-160 in particular shares some chemical characteristics with the volcanic rocks, having high Nb/Y and relatively low TiO_2 and P_2O_5.

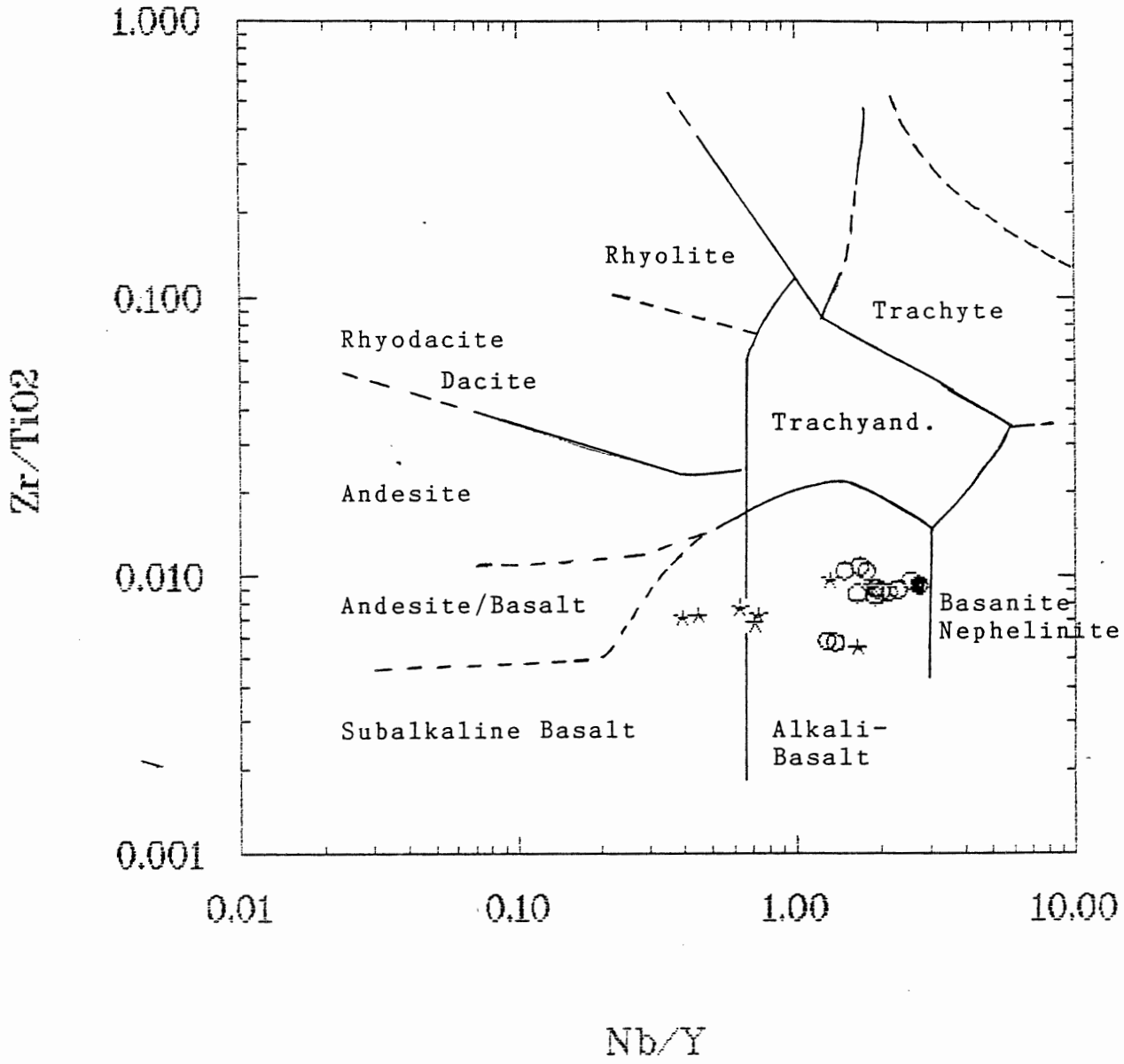

Figure 10. Chemical Classification of Audhild Igneous Rocks.
○ = Basalt, ● = Volcaniclastic,
★ = Intrusive.
Zr, TiO_2, Nb, Y in ppm.
Fields after Winchester and Floyd, 1977.

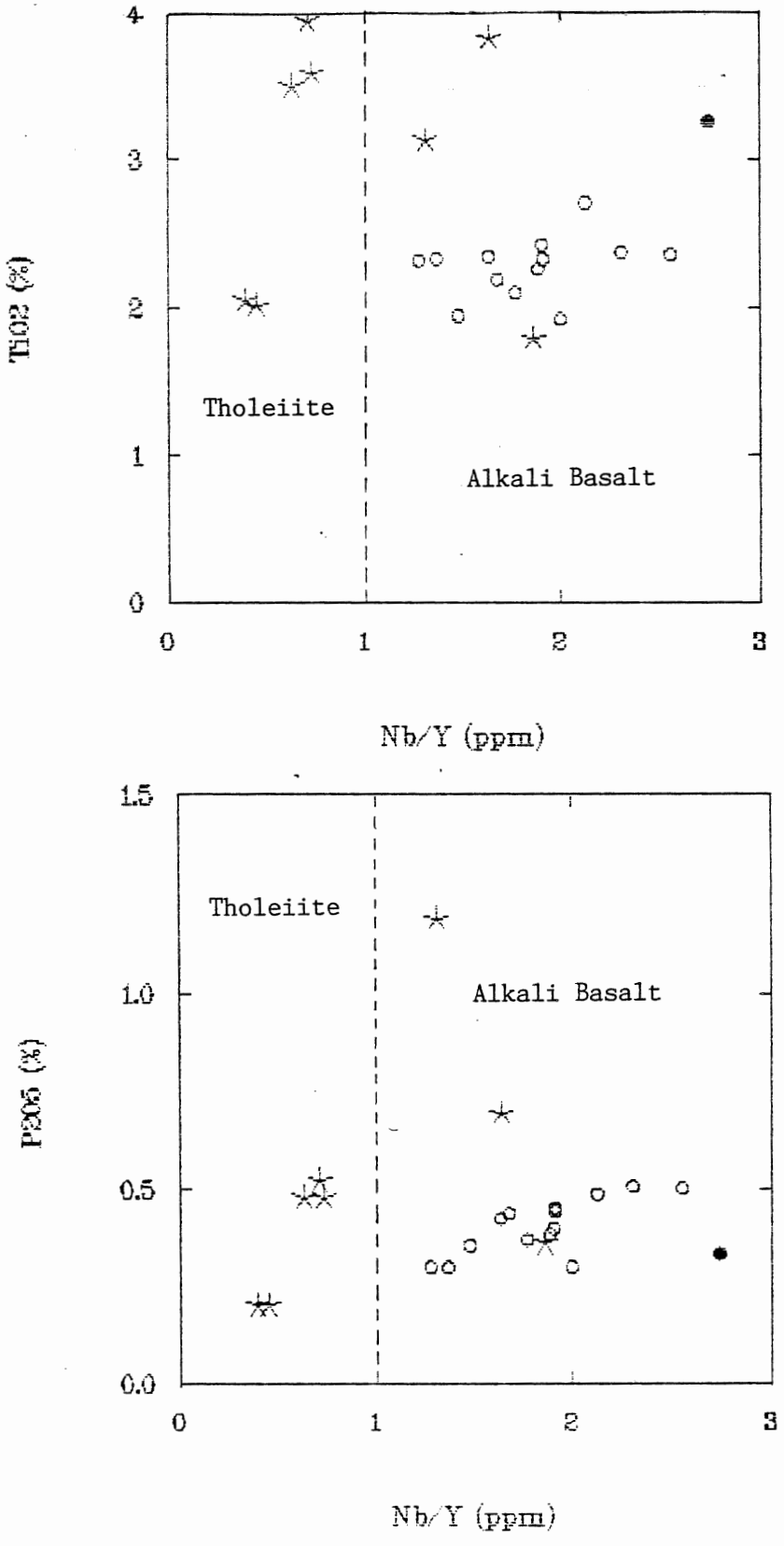

Figure 11. TiO_2 and P_2O_5 vs. Nb/Y.
Values for EL 87-160 Plot With Those for Basalts.
○ = Basalt, ● = Volcaniclastic, ✳ = Intrusive.

In general, chemical distinctions between intrusives do not correspond to mineralogical and textural differences reported in section 3.2.

4.3.2 Rare Earth Elements

The rare earth elements (La - Lu) are all ordinarily present in magmatic systems as trivalent ions, except for europium, which commonly exists in the divalent state under conditions of relatively low oxygen fugacity (Duchesne, 1983). In combination with the constant 3^+ ionic charge, the inverse relationship between ionic radius and atomic number produces a systematic change in hygromagmatophile character within the series. La and Ce (light REEs) are considered hypermagmatophile elements or H elements (Allegre and Minster, 1978), while the smaller, heavier lanthanides (e.g. Yb, Lu) are included among the magmatophile elements (M elements) that are not so strongly concentrated in the melt fraction. This systematic variation makes REEs of great value in petrologic and petrogenetic studies of igneous rocks.

When concentrations of rare earth elements are normalized to their estimated abundances in the primitive mantle (Taylor and McLennan, 1985), they are readily presented as functions of their atomic number (figure 12). The resultant patterns may be useful in distinguishing basalt types and in ascertaining probable mode of origin for igneous rock suites. Normalized REE concentrations in analyzed basaltic flow units fall within narrow ranges (figure 12d) and the six patterns are very similar, with EL87-169 being somewhat enriched in light REEs and relatively depleted in heavier

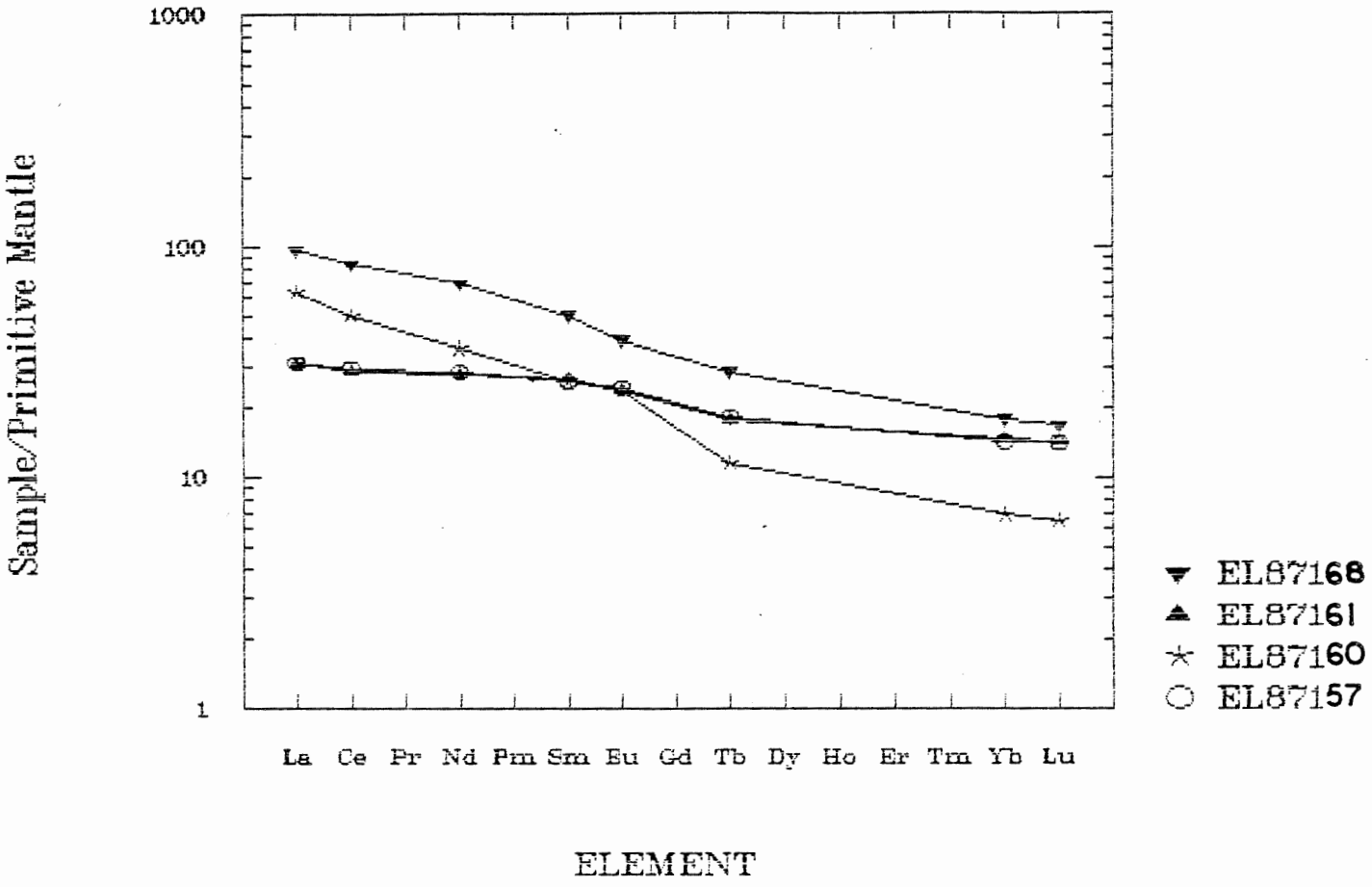

Figure 12a. Normalized REE Patterns for Intrusive Rocks

Audhild Basalts

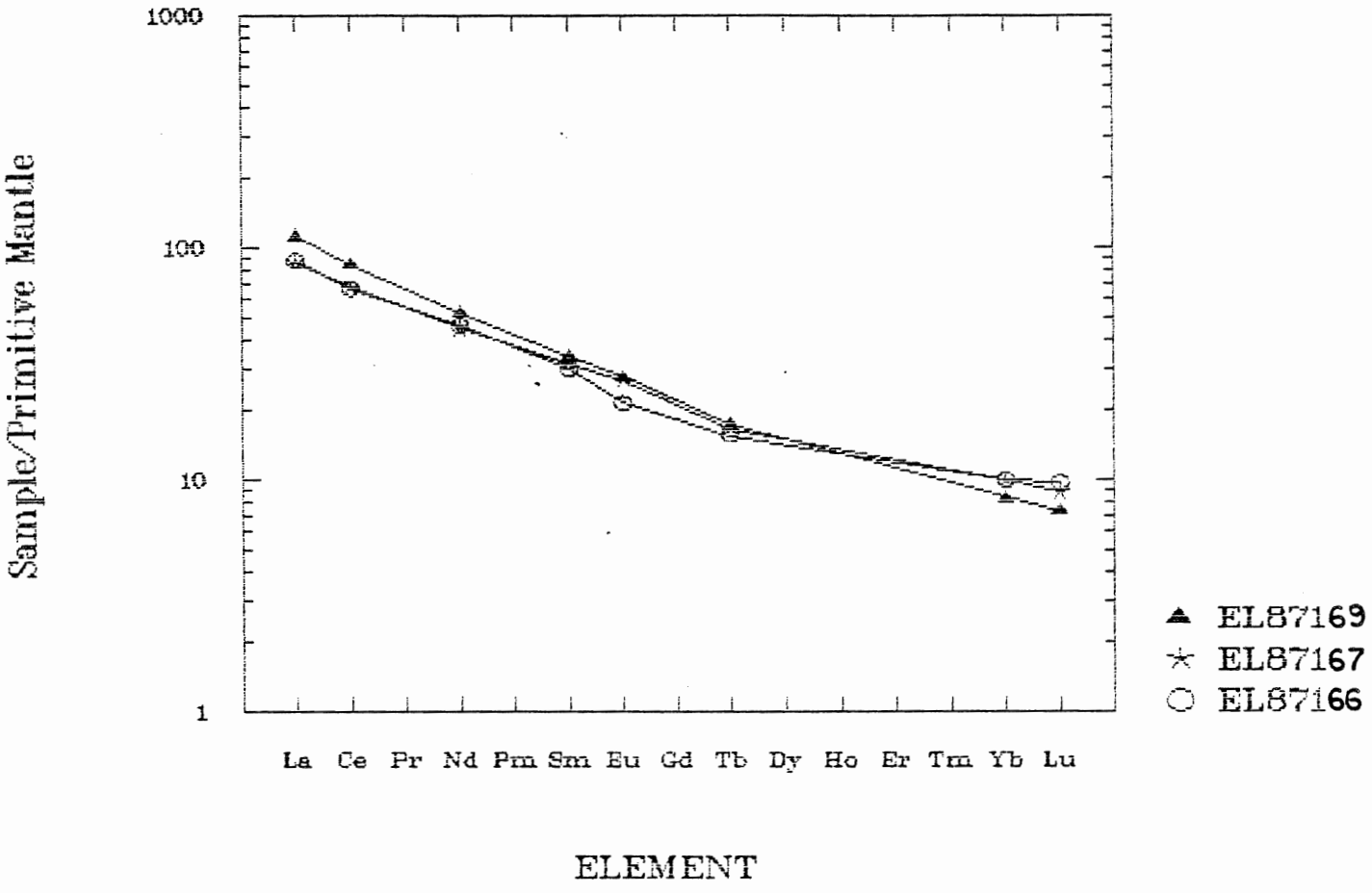

Figure 12b. Normalized REE Patterns for 3 Basalt Samples.
EL 87-166 and EL 87-167 are from the same flow unit.

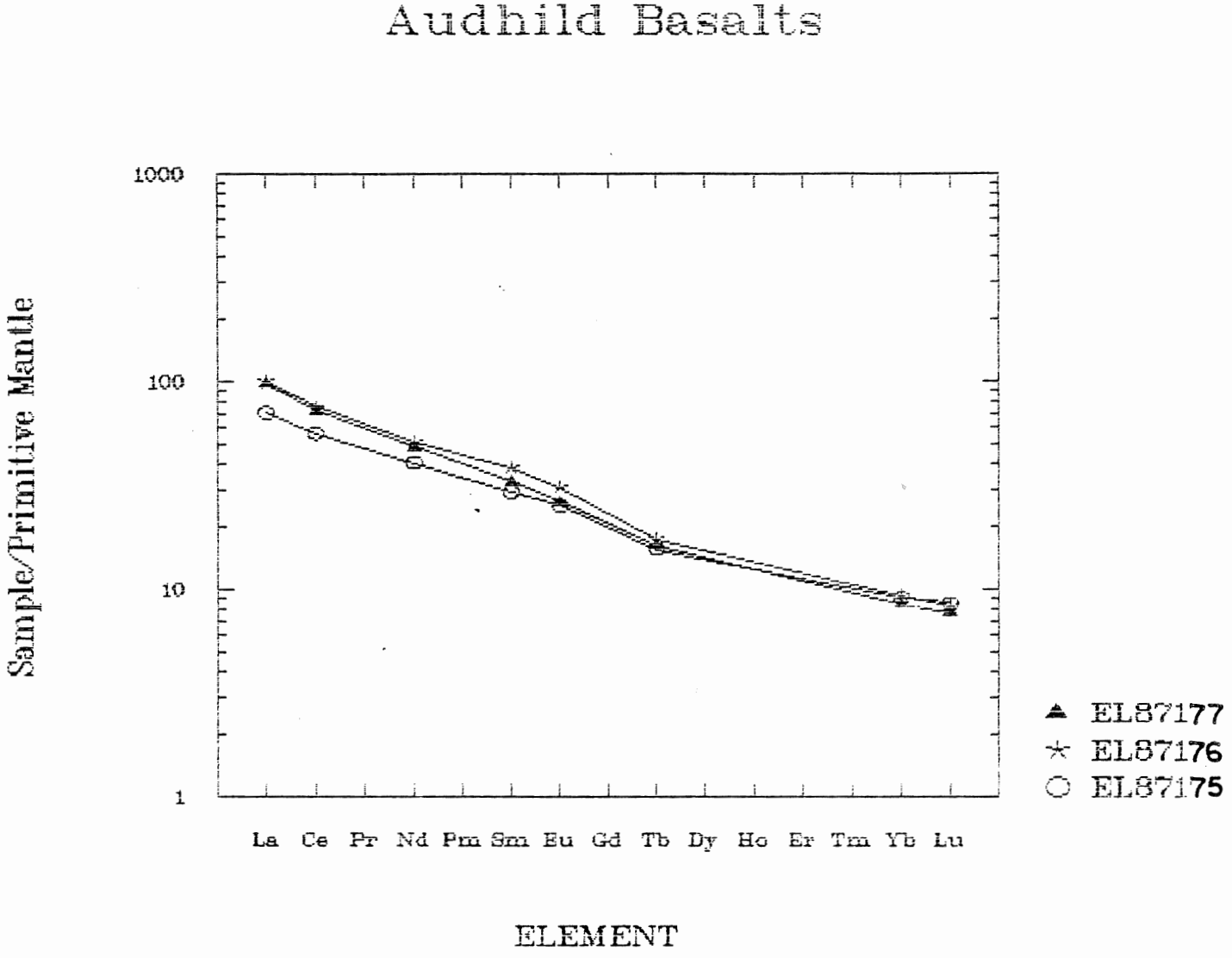

Figure 12c. Normalized REE Patterns for 3 Basalt Samples, Including EL 87-176 - The Least Altered Basalt.

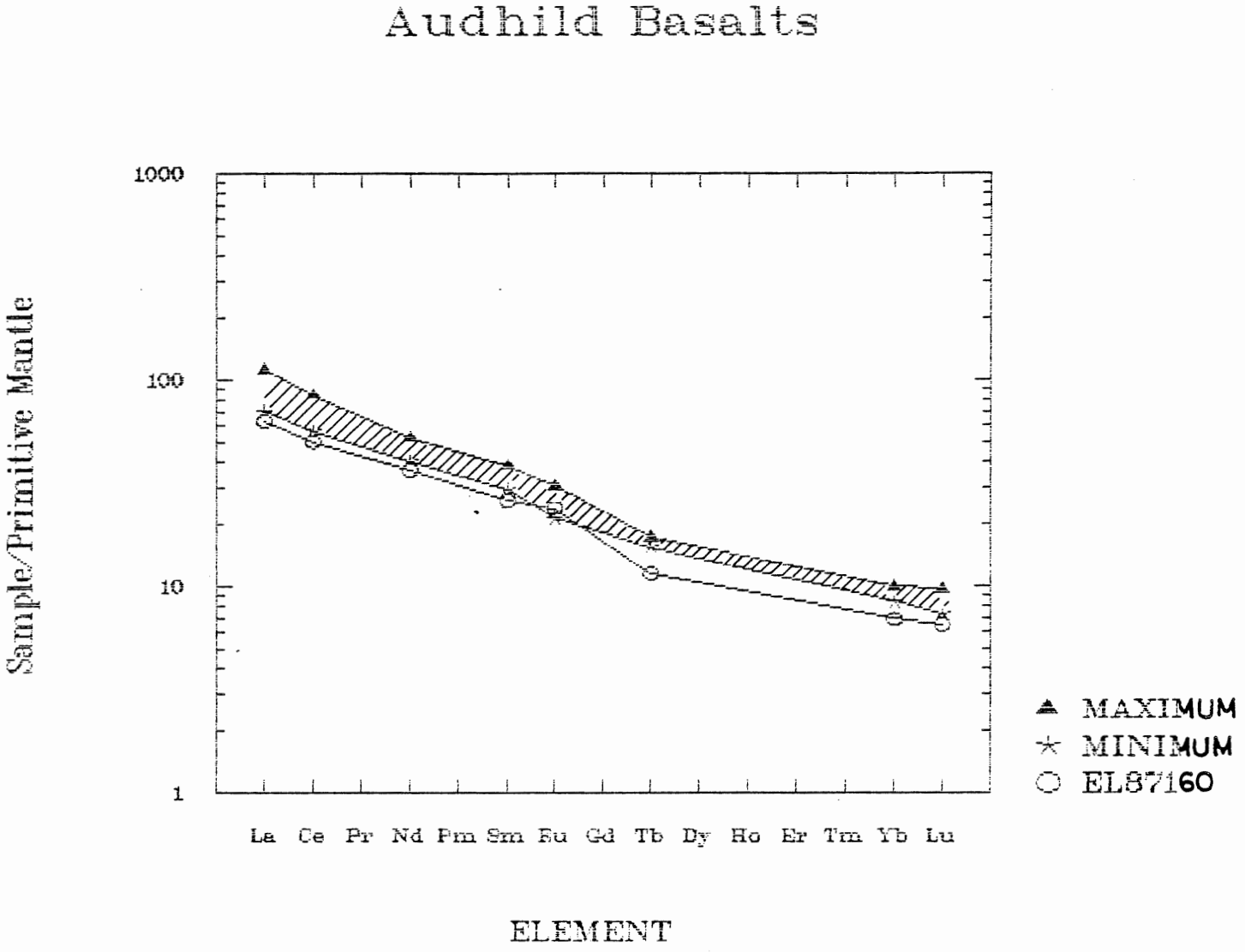

Figure 12d. Summary Diagram for REE Patterns of Alkalic Rocks. The ruled portion indicates the range of normalized REE values for basalt flows.

elements of the series. This constancy of pattern suggests that REEs have not been mobilized, yet the sum of REEs shows a poor correlation with the chosen index of fractionation, Zr. The correlation (table 4) with Nb, another incompatible element, is much better.

The intrusive rocks are readily separable from extrusives by their REE contents. Sample EL87-160 displays a pattern that parallels that of the volcanics, but it is distinct in having lower levels of all analyzed REEs except europium. Of the intrusive rocks that were determined to be alkaline, this is the only one that was submitted for REE analysis. All alkaline rocks have normalized LREE/HREE (La/Lu) ratios between 9 and 12. The tholeiitic intrusives are characterized by patterns that are much less steep than those for alkaline rocks, with La/Lu between 2.9 and 5.5, and they conform to patterns generally observed for tholeiitic basalts or andesites (Taylor and McLennan, 1985).

4.4 Primary Variations

Elements that are sensitive to changes in crystal/melt proportions are potentially useful in determining the processes of magma generation and differentiation that produce the observed chemical composition of a volcanic suite. These sensitive elements include Cr and Ni which have very high bulk distribution coefficients and are concentrated in residual solids during partial melting or in early crystals during fractionation. The plot of Cr versus Ni (figure 6) that was previously presented as an effective

discriminator between intrusives and extrusives also contains useful information on the processes that generated these rocks. If the series of basalt flows was erupted from a body of magma that was crystallizing Cr- and Ni-enriched minerals (e.g. olivine, clinopyroxene, chromite - the typical early phases), a strong linear trend toward (0, 0) would be developed. No such trend is evident and the Audhild basalts are apparently not simply related by a process of crystal fractionation. If any intrusives are derived by fractional crystallization from the magma that produced the flows, then no intermediate products are observed. Because levels of Cr and Ni are very sensitive to the presence of phenocrysts, strictly speaking only aphyric rocks should be used in examining the evolution of a volcanic suite (Minster and Allegre, 1978). In fresh lavas, it might be possible to keep account of phenocryst composition and volume, and if this were possible in the Audhild volcanics, a trend might become evident.

Hypermagmatophile (H) and magmatophile (M) elements (Allegre and Minster, 1978) are strongly partitioned into the melt phase and their concentrations will vary according to the proportion of melt generated or remaining. In a fractional process of melting or crystallization, the developing phase (crystals or liquid respectively) never amounts to a significant proportion of the total system before it is removed. Typically, the distribution coefficient between solid and coexisting melt for an M element is $D^M = 0.1$; D^H (the coefficient for an H element) can be approximated to zero such that the ratio of H in the liquid phase (defined as

C^H_l) to H in the total system (C^H_o) is given by $\frac{C^H_l}{C^H_o} = \frac{1}{f}$ with melt fraction = f. For an M element, the ratio is $\frac{C^H_l}{C^H_o} = f^{(D-1)}$, since D is not negligible. When f is near 1 (fractional crystallization), the two relationships are essentially equivalent and the concentrations of H and M elements vary in the same way. The behaviour of H and M elements is not similar during fractional melting (f very small). Magmas are unlikely to separate from their parental solids until some substantial portion of the system has melted. H and M elements behave differently under these conditions of batch melting. Graphical methods for identifying the processes of batch melting, fractional melting, and crystallization are summarized in Minster and Allegre (1978). Differentiation by fractional crystallization yields a straight line with intercept (0, 0) and slope=1 on either a C^M vs C^H or C^H vs C^H plot. During melting processes, however, the H element is more strongly partitioned into the melt and a lower slope is produced on C^M vs C^H. When C^H/C^M is plotted against C^H, crystal fractionation is identified by the constant C^H/C^M ratio that generates a horizontal line. This constant ratio is the result of the similar behaviour of H and M elements during fractional crystallization. Batch partial melting produces lower C^H/C^M because C^H decreases more rapidly than does C^M with increasing melt fraction.

The plots presented in figure 13 (13b in particular) show trends which suggest that the Audhild basalts are related by a process of partial melting, not crystal fractionation. The distribution coefficient for scandium in clinopyroxene is about 3 (Allegre et al., 1977; Basaltic Volcanism Study Project, 1981),

but when Sc is plotted as a function of Zr (an M element) (figure 13c) it behaves as an H element. In combination with the high Cr concentrations, the behaviour of Sc offers a further argument against fractional crystallization of clinopyroxene. For the Permian Esayoo lavas, an inverse relationship between Sc and Zr is evident, suggesting the occurrence of clinopyroxene fractionation within that suite. The lack of a negative europium anomaly is evidence that fractionation of plagioclase has not played a role in the genesis of the Audhild volcanics, although the incorporation of Eu into feldspar is dependent upon oxygen fugacity, which is an unknown factor.

4.5 Tectonic Discrimination

4.5.1 Whole Rock Composition

The relatively immobile elements have been proposed by several authors to be useful in determining the magmatic affinity and tectonic setting of metabasalts which cannot be classified by mineralogy and major element content. A Ti-Zr-Y ternary plot distinguishes between basalts generated in within-plate and mid-ocean ridge settings (Pearce and Cann, 1973). All Audhild volcanic, volcaniclastic, and intrusive rocks are in or adjacent to the field for within-plate basalts (figure 14). The Nb-Y-Zr plot (Meschede, 1986) has been divided into fields that further distinguish within-plate tholeiite from within-plate alkali basalt. The extrusive rocks (basalt and pyroclastic) plot as a cluster within the alkali basalt field (figure 15), while 5 intrusives fall in the overlap field of tholeiitic and alkaline rocks. Intrusive

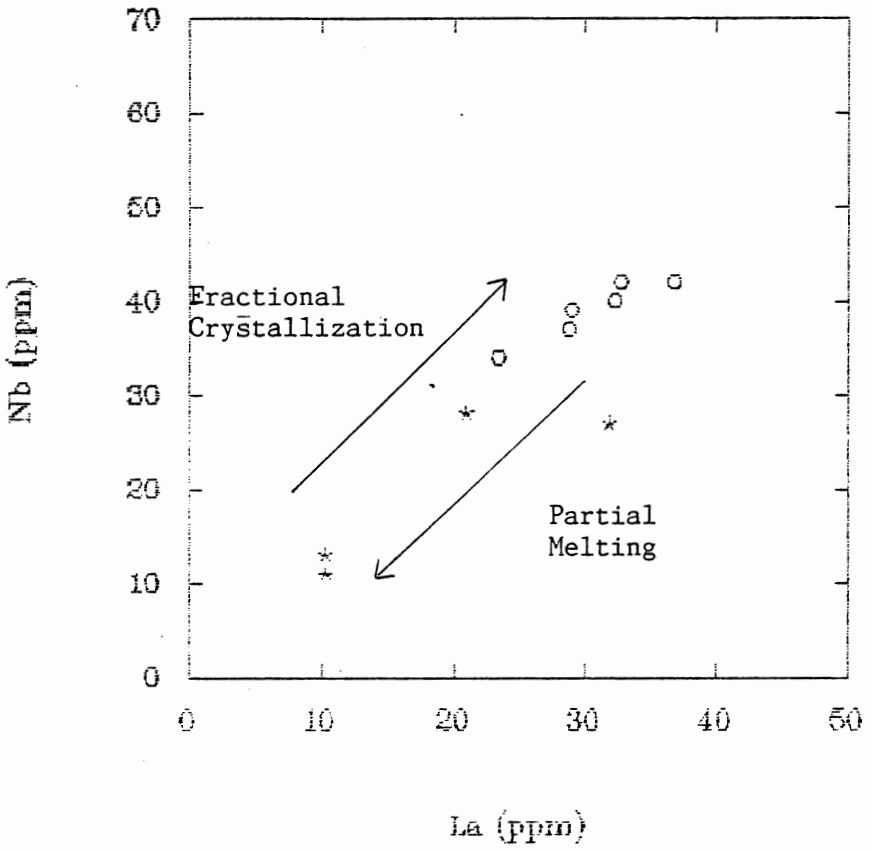

Figure 13a Nb (ppm) vs. La (ppm). An Example of C^H vs. C^H

★ = Intrusive

o = Extrusive

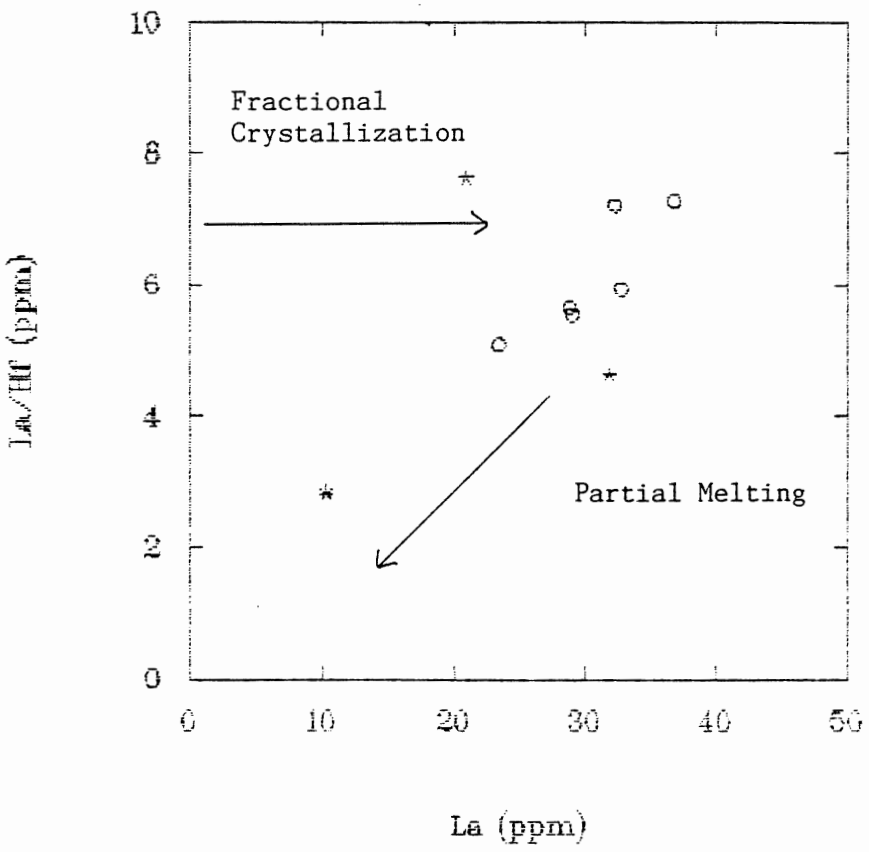

Figure 13b. La/Hf (ppm) vs. La (ppm). An example of C^H/C^M vs. C^H.

★ = Intrusive

○ = Extrusive

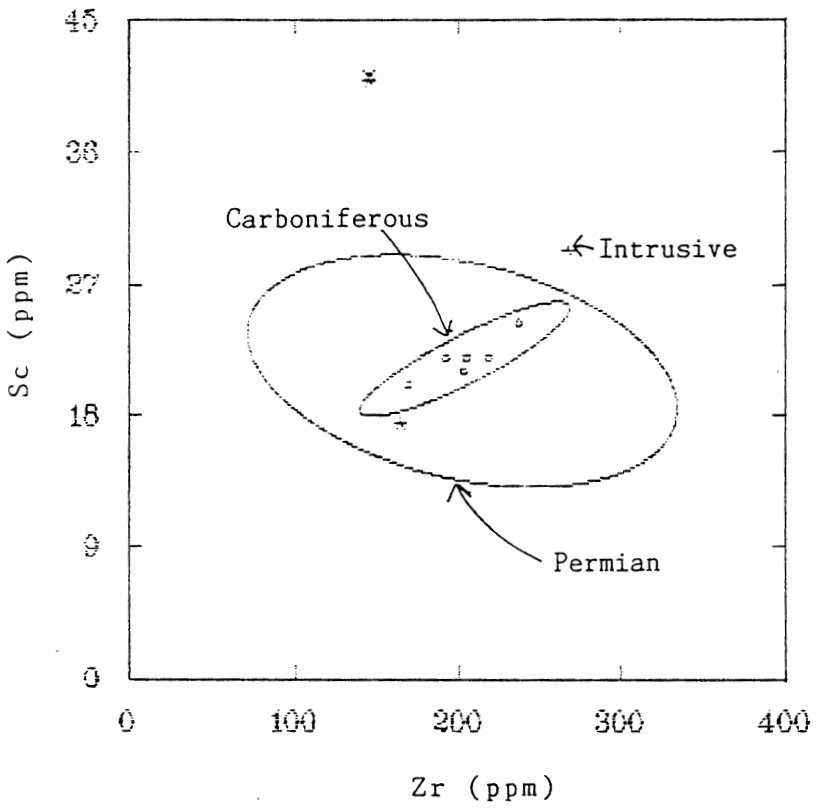

Figure 13c. Contrasting Behaviour of Scandium in Auhild Extrusives • , Auhild Intrusives ✶ , and Permian Extrusives.

rocks that were shown to have alkaline affinities (section 4.3) plot in the alkali field.

4.5.2 Mineral Composition

Discrimination diagrams based on the Ti, Ca, Na, Cr, and Al content of intact igneous clinopyroxenes have also been developed (Leterrier et al, 1982). Clinopyroxene is a common phase in basaltic suites and has an affinity for titanium. Phenocrysts of clinopyroxene from alkali basalts are typically higher in atomic proportions of Al and Ti, and have lower Si than other basalt types (Allegre et al.,1977). The intrusives that have alkaline affinity (section 4.3) are those that have high TiO_2 in clinopyroxene (section 3.4). The clinopyroxene-bearing flow is classed as alkaline on the basis of stable trace element ratios, but titanium levels in augite from that sample are near those of tholeiitic intrusive rocks. Plots of Ti and Al versus Si (figure 16a, 16b) fail to separate alkaline extrusive from tholeiitic intrusive rocks. Pyroxenes from alkaline intrusives are relatively enriched in both Ti and Al, and analyses fall within a restricted range on both diagrams, but this range overlaps with those for other rock types.

Separation of alkali and other basalt types by use of a Ti versus Ca + Na diagram has been proposed by Leterrier et al. (1982). Those intrusive rocks previously designated as alkalic or tholeiitic are again identified as such, but the discriminant diagram (figure 17) fails to classify the alkaline flow (EL 87-176). The division between alkaline and tholeiitic is not a sharp

14 Basalts

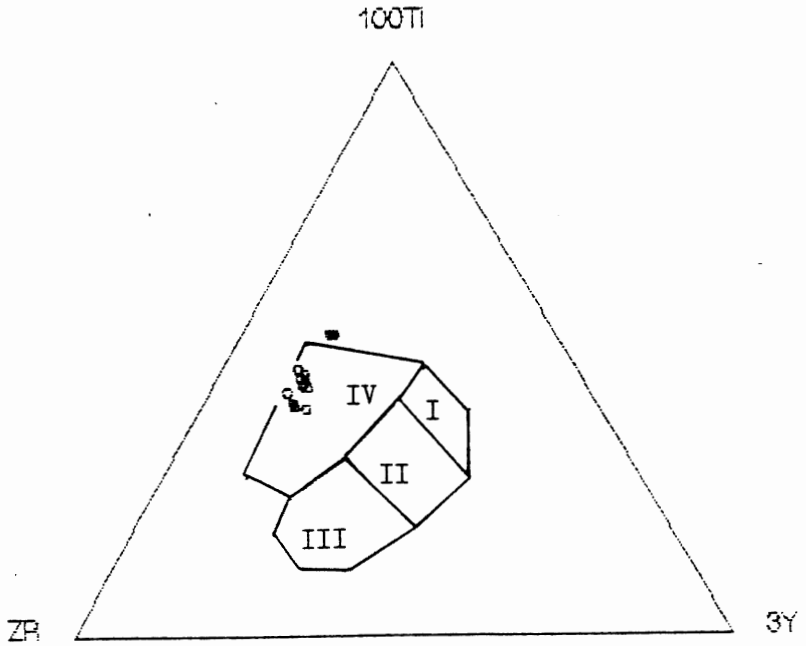

8 Intrusives

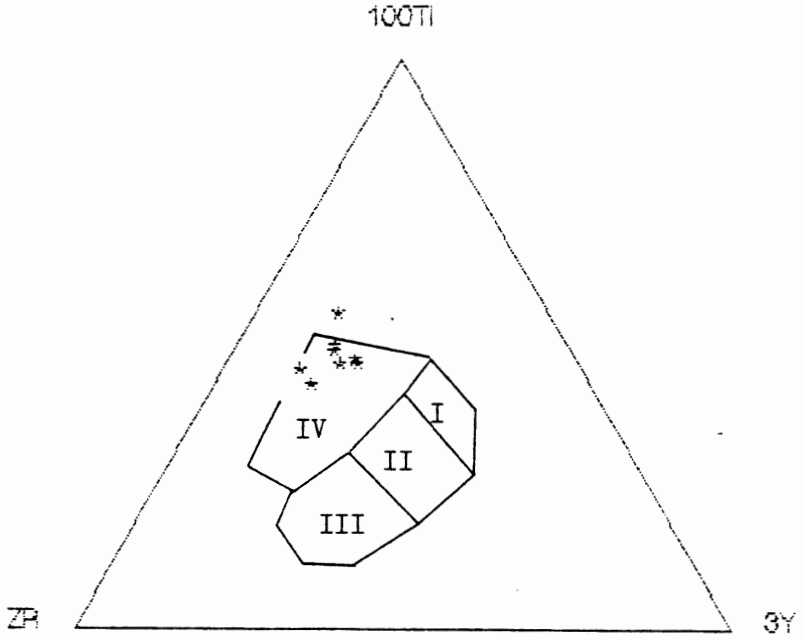

Figure 14. Discrimination diagrams using Ti, Zr, and Y with fields from Pearce and Cann, 1973. I, II = Low-potassium tholeiites, II, III = Calc-alkali basalts, IV = Within-plate basalts. 100 Ti = 100 x TiO_2 in %, 3Y = 3 x y in ppm, ZR = Zr in ppm.

14 Basalts

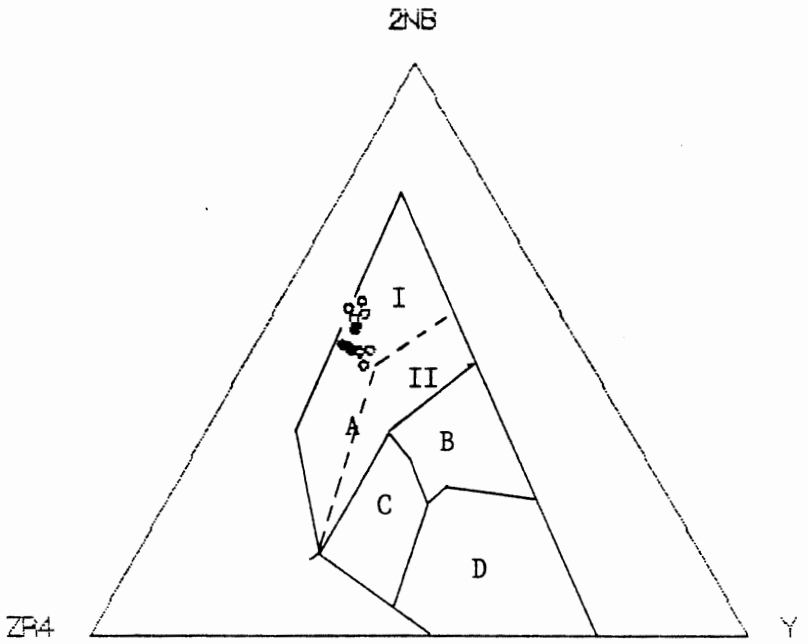

8 Intrusives

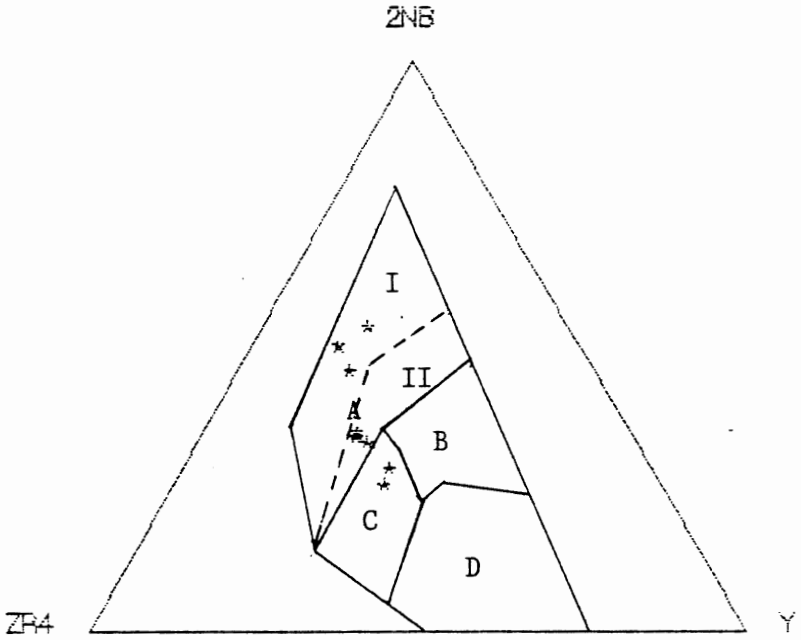

Figure 15. Discrimination Diagrams Using Nb, Y, and Zr with Fields from Meschede, 1986. AI, AII = Within-plate alkali basalt, AII, C = Within-plate tholeiite, B,D = MORB, C,D = Volcanic Arc Basalts. 2NB = 2 x Mb in ppm., Y = Yttrium in ppm., Zr4 = Zr/4 in ppm.

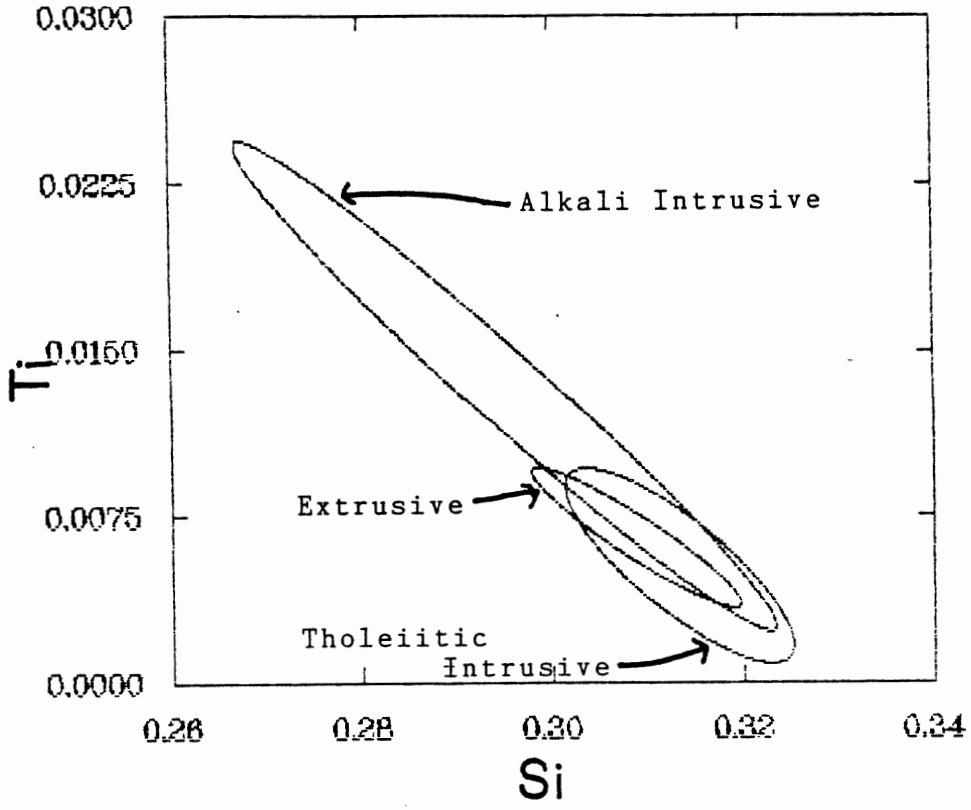

Figure 16a. Atomic Ti vs. Atomic Si (per 1.0 oxygen atoms) in Clinopyroxenes. Elliptical Fields Include 85% of Analyses for Indicated Rock Types.

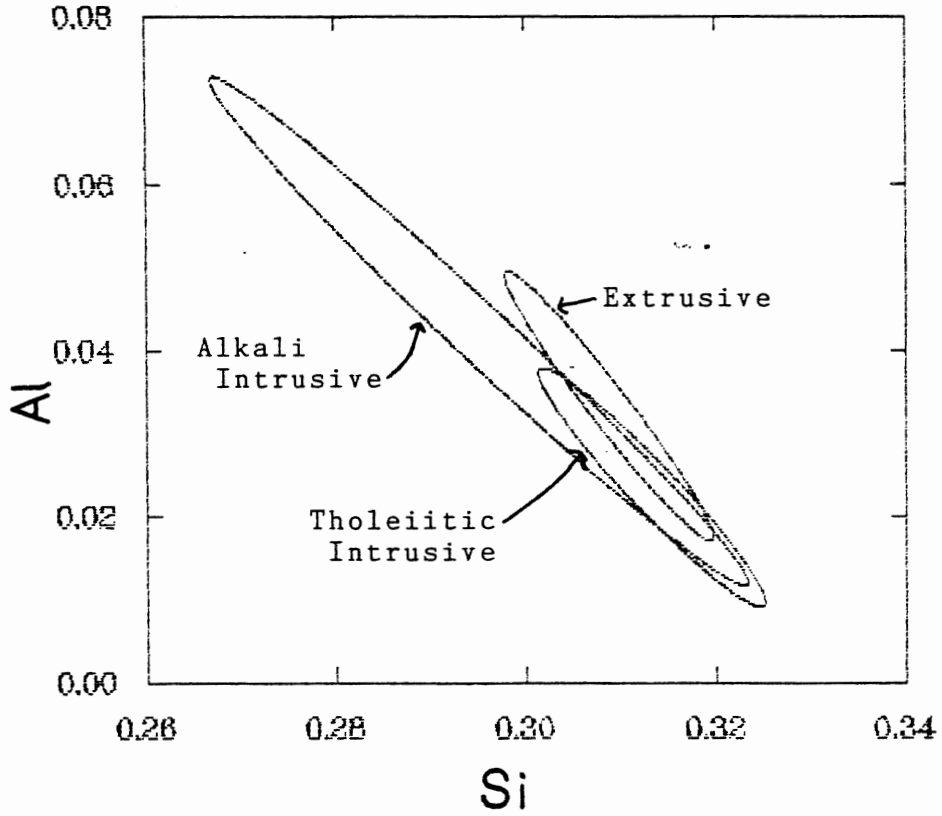

Figure 16b. Atomic Al vs. Atonic Si (per 1.0 oxygen atoms) in Clinopyroxenes. Elliptical Fields Include 85% of Analyses for Indicated Rock Types.

one, however. A degree of overlap does exist such that the division can ordinarily be made only with 80% confidence (Leterrier et al.,1982). Clinopyroxene in this sample is not host to a significant part of the TiO_2 reported in the whole rock analysis. Titanium is partitioned into ilmenite (where TiO_2 is an essential component) more strongly than into clinopyroxene (Allegre et al., 1977). The crystallization sequence of a magma is influenced by many factors and the crystallization of ilmenite (containing only ferrous iron) or magnetite (containing ferric iron) may be a function of oxygen fugacity in the melt.

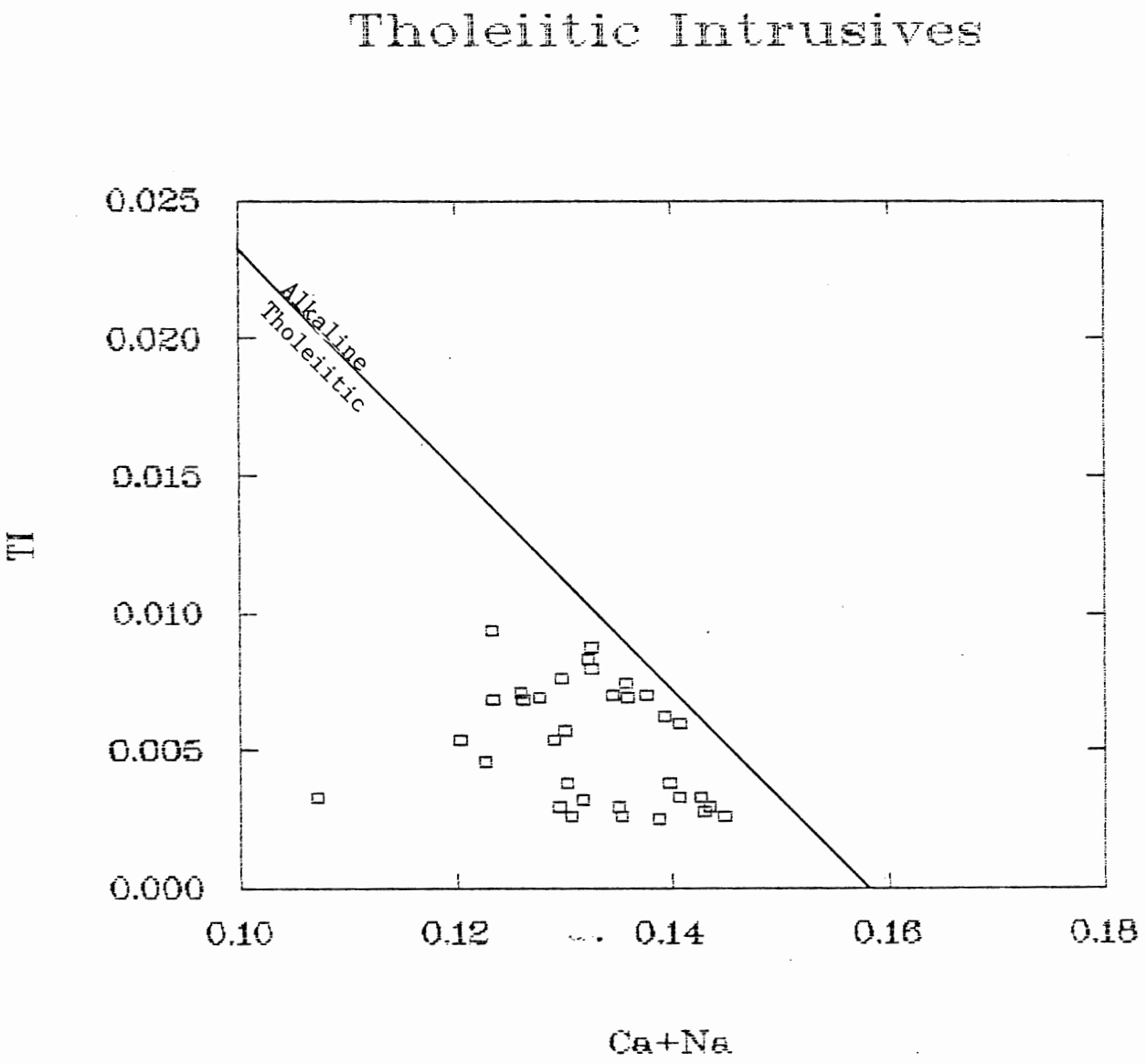

Figure 17a. Discriminant Diagram Based on Pyroxene Composition. Applied to intrusive rocks previously indicated to be tholeiitic or subalkaline.

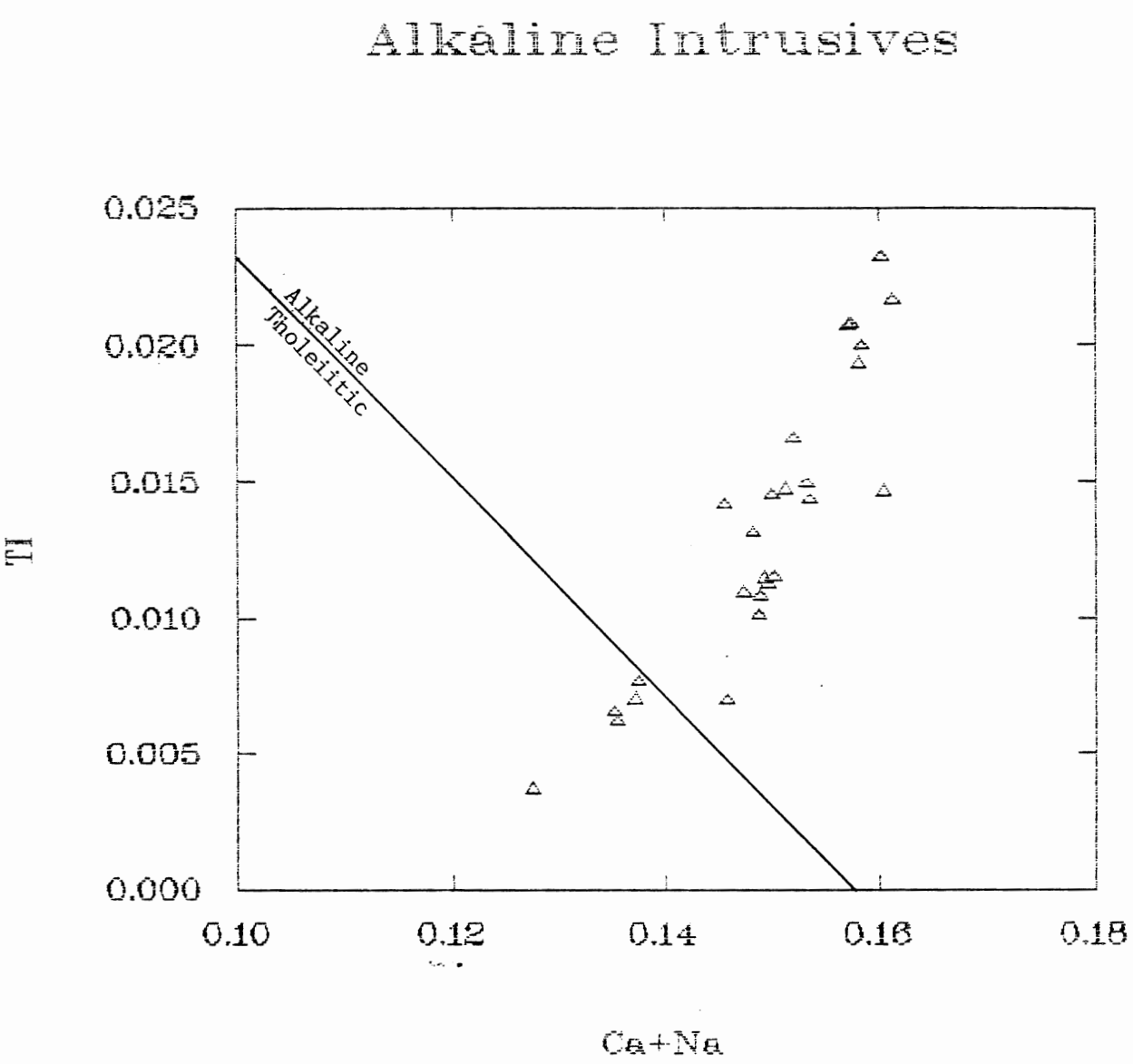

Figure 17b. Discriminant Diagram Based on Pyroxene Composition. Applied to intrusive rocks previously indicated to be alkaline.

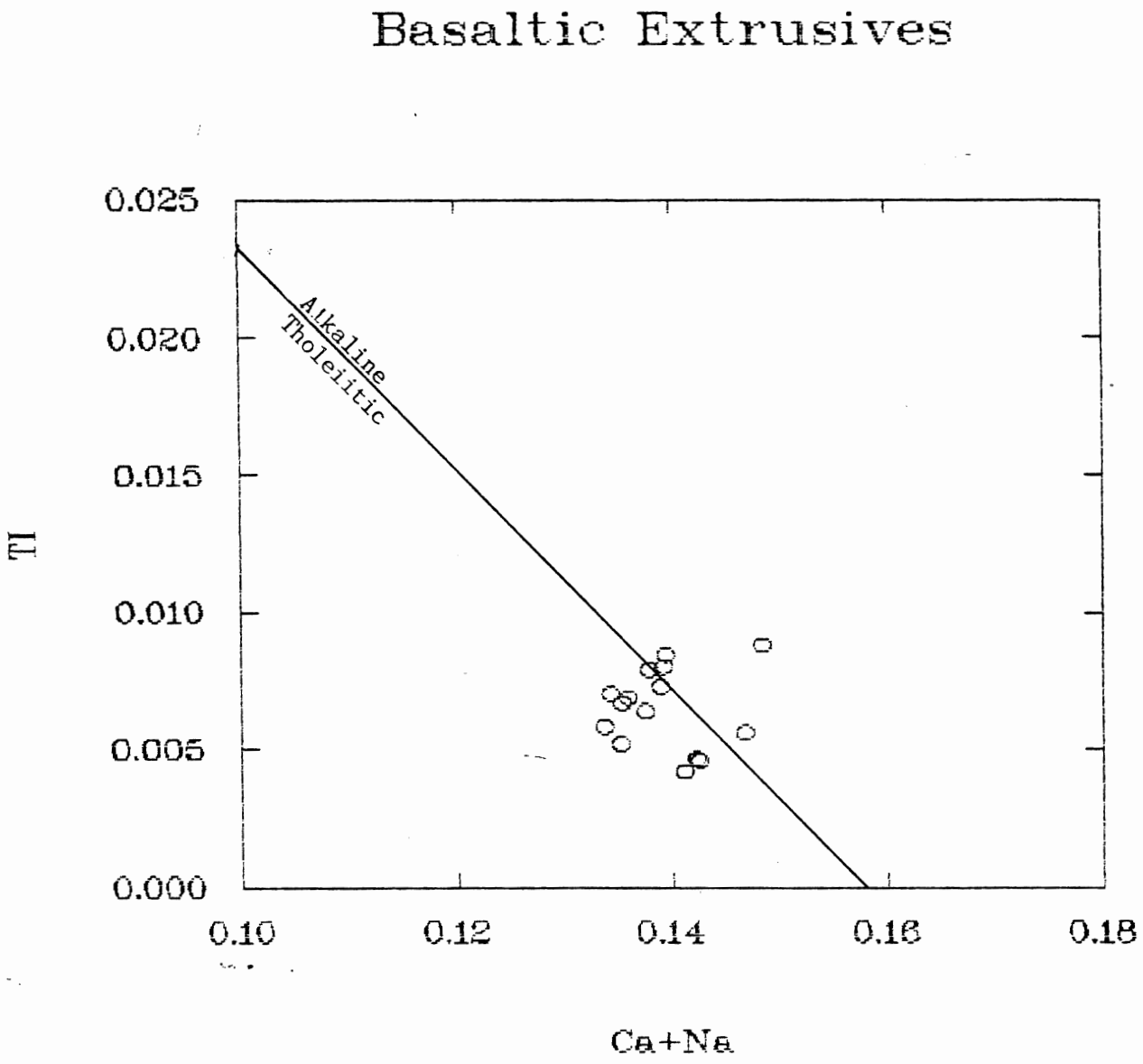

Figure 17c. Discriminant Diagram Based on Pyroxene Composition: Analyses from the pyroxene-bearing basalt flow lie on both sides of the division between alkaline and tholeiitic rocks.

5. DISCUSSION

5.1 Petrogenetic Implications of Basalt Chemistry

The variations in trace element contents of the Audhild volcanic rocks suggest that they are the product of varying degrees of partial melting rather than crystal fractionation. Chemical composition is broadly consistent with generation by small to moderate degrees of melting [3 to 30% (Allegre et al.,1977)] of an upper mantle source. Primary magmas derived from the mantle are expected to contain 300 ppm or more Ni (Allegre et al.,1977; Basaltic Volcanism Study Project,1981). The high contents of Cr (mean 391 ppm) and Ni (mean 226 ppm) and the lack of fractionation trends within the suite suggest that they approach primary mantle melt compositions. Cr and Ni are at the low range of estimates for primitive, unfractionated magmas, but since these two elements are strongly retained in the residual solids they will be somewhat lower in the liquid at smaller degrees of melting (<10%). Evidently, there has been little removal of magnesian minerals such as olivine and pyroxene, so the MgO content of the basalts (mean=6.4 wt %) might be considered unusually low. If Mg has been removed during alteration, however, then this low level is not a primary characteristic of the lavas. Chlorite is present in all basalt samples in this study, and if it is host to a significant part of the whole rock MgO, then magnesium has been mobile, at least on the scale of individual mineral grains. Alternatively, Mg (along with Ni and Cr) may have been left in mantle minerals when melts were generated. The presence of plagioclase, pyroxene,

and (relict) olivine phenocrysts requires that some crystallization did in fact take place prior to eruption, but apparently there was little segregation of crystals and melt. If the initial melts contained 300 ppm Ni, then removal of approximately 3% olivine [D for nickel in olivine = 13 (Allegre et al., 1979)] will reduce Ni in the residual liquid to 200 ppm. Primary mantle melts generated near the solidus can contain less than 10% MgO (Takahashi, 1986); reduction from 9% MgO to 6% is achieved by removal of 6.8% which contains 50% MgO by weight. The lack of fractionation trends for Cr and Ni could be explained by invoking a process whereby all lavas fractionated (probably olivine and spinel) to approximately the same degree. The trace element ratios that show partial melting trends (e.g. Ta/Zr, La/Hf;figure 13) argue against the presence of any single parent melt and there is no reason to suspect such a uniform process of crystallization acting in a succession of many melts. It is important to realize, however, that conditions (cooling) did exist during the ascent of magmas through the crust that would allow or promote partial crystallization. Chemical trends suggest that melts were generated independently and erupted periodically onto the surface without the establishment of a permanent magma reservoir under the developing basin.

Concentrations of the highly incompatible light REEs (La, Ce) are elevated by a factor of about 100 over mantle composition (figure 12). This degree of enrichment is consistent with melting of only a few per cent of a primitive mantle source. The net partitioning of H or M elements between solid and liquid depends

on both the nature and quantity of minerals in the solid. Even a mineral that has an extreme affinity for a certain element cannot strongly deplete that element in the coexisting melt if the solid phase constitutes only a minor fraction of the entire system. Minster and Allegre (1978) give bulk distribution coefficients of REEs for melts in equilibrium with various mantle mineral assemblages. In particular, garnet and clinopyroxene retain or take up heavy REEs (Duchesne, 1983). By application of the coefficients presented by Minster and Allegre (1978, the LREE/HREE ratio of the Audhild basalts indicates that the melts were in equilibrium with a garnet-, clinopyroxene-, and olivine-bearing assemblage. The likely source rock is thus identified as a garnet lherzolite.

A different source is indicated for the tholeiitic dykes, which do not yield high LREE/HREE ratios. These rocks may have been produced from or equilibrated with a non-garnet-bearing assemblage (Duchesne, 1983). Low Cr and Ni in all analyzed dykes implies that they have undergone substantial crystal fractionation, and are therefore at least one further step removed from their original source. The difficulty in determining source characteristics increases with the number and complexity of processes that have acted upon the melts.

5.2 Tectonic Implications

Field observations establish the tectonic setting of the Audhild Formation as a dominantly continental one. The position of the subaerially erupted basaltic flows within a sedimentary

basin fill sequence supports the contention that they are a product of the rifting and crustal extension that produced the Sverdrup Basin. During extension of the continental lithosphere, adiabatic upwelling of the mantle generates little melt until thinning reaches of exceeds 100% (McKenzie and Bickle, 1988; figure 18), and the occurrence of volcanic rocks near the basin margin where stretching was apparently much less (figure 19) introduces the possibility of heterogeneous crustal structure or uneven distribution of crustal thinning. The large scale faults that are associated with basin margins can induce heterogeneous decompression of the mantle, and will also provide conduits to the surface for any melt that is generated. It is unlikely that 100% thinning was achieved over any large region in the early stage of basin development when the Audhild Formation was erupted. Early volcanic activity may therefore have been very localized and highly diachronous. Basaltic rocks within the Borup Fiord Formation on Axel Heiberg Island may be as much as 10 Ma older than the Audhild sequence of flows (Trettin, 1988). Stephenson et al. (1987) note that inconsistencies arise between the predictions of a model based on a single rift event and the observed sedimentation patterns within the Sverdrup Basin. The development of unconformities in areas of relative uplift throughout the early stages of basin subsidence is evidence for a long (but probably not continuous) history of rifting. It remains unresolved whether sufficient diachroneities and heterogeneities are evident in the rifting process to account for the observed distribution (both temporal and spatial) of volcanism and sedimentation or whether special

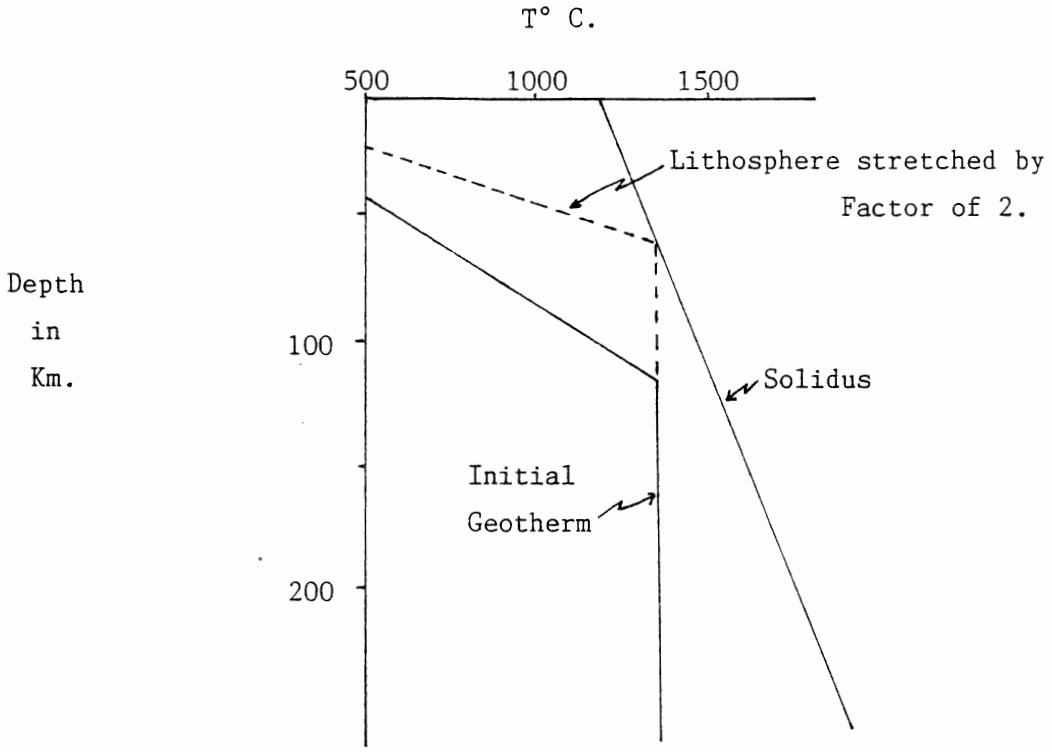

Figure 18. Initiation of Mantle Melting by Lithospheric Extension. The geotherm intersects the solidus after the lithosphere is stretched and thinned. Geotherm from McKenzie (1984); Solidus from Green and Ringwood (1967).

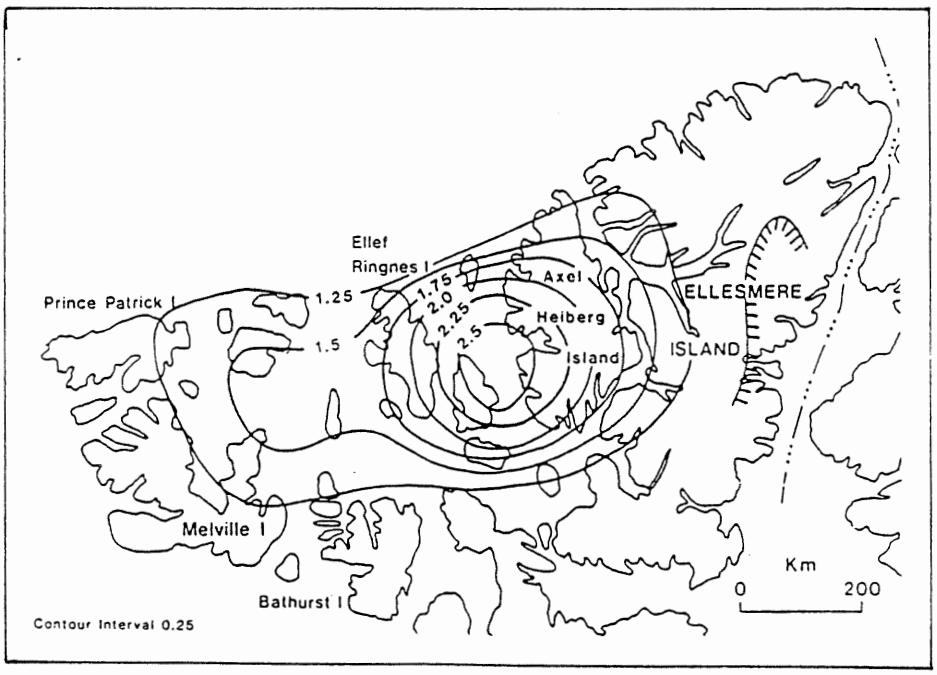

Figure 19. Geographic Distribution of Beta-values in Sverdrup Basin. From Stephenson et al. (1987).

conditions such as elevated mantle temperature are required.

5.3 Multiple Phases of Magmatism in the Sverdrup Basin

Analytical data for three samples of basaltic dykes plot (figures 9, 10, 11) near or on trends with the extrusives (both volcaniclastic and basaltic). These rocks (EL 87-159, EL 87-160, EL 87-173) are potential candidates as intrusive equivalents of derivatives of the Audhild basalts. No intrusive contains the high levels of Cr or Ni that typify the extrusives, so if any of the two rock types share a genetic link, a considerable degree of crystal fractionation must have taken place. Although sample EL 87-159 is TiO_2-rich, due to the high modal abundance of titanaugite, it and EL 87-173 generally extend the linear trends of the extrusive rocks (figure 9). Enrichment in the incompatible elements is consistent with derivation by fractional crystallization from a magma like that which produced the basalt flows prior to fractionation. Nb/Y, the index of alkalinity (figures 10,11), is not expected to vary greatly during crystal fractionation. EL 87-160 has the closest chemical affinity to the extrusive rocks because it is not enriched in incompatible elements (Ti, Y, Zr, Nb, P, REEs) (figures 9,12). It must be highly fractionated, however, especially in terms of Cr and Ni, if it has been derived from the same magma as the volcanic rocks. This lack of enrichment can be explained, at least in part, by considering the mineralogy and texture of the rock. El 87-160 is made up of 40% plagioclase phenocrysts that crystallized with the exclusion of H and M elements (including europium). The bulk rock composition does not reflect the partitioning of incompatible

elements into the relatively small volume represented by the groundmass. There is insufficient evidence to rule out the possibility that alkaline intrusives evolved from magmas that generated the flows.

In contrast to the Audhild Formation, Permian volcanics of the Sverdrup Basin do show trends of evolution by fractional crystallization (Cameron, in prep.; figures 6, 13c). Quantities of melt sufficient to establish magma chambers seem to have been generated by that time. The Audhild basalts are the products of magmas that have some features in common with a parental melt for the Permian Esayoo basalts. It is unlikely, however, that the Esayoo magmas evolved from those represented by the Audhild basalts, because rifting and melt generation must have been continuous or at least episodic throughout the Late Carboniferous and Permian. Isotopic comparisons of the Audhild and Esayoo volcanics might be useful in determining whether the magmas of the two volcanic episodes were derived from similar mantle sources or whether the mantle beneath the Sverdrup Basin during the Permian had been substantially depleted by earlier melting. The role of crustal assimilation can also be assessed by isotopic studies.

6. CONCLUSIONS

Field and petrographic observations indicate that the metavolcanic rocks of the Audhild Formation are spilitized basalts and associated volcaniclastic rocks, but mineralogical and major element indicators of their original igneous affinities are obscured by the extensive development of the secondary mineral assemblage calcite + chlorite ± zeolites ± silica. This alteration assemblage was developed by introduction and circulation of fluids and mobilization of rock components soon after eruption and during subsequent burial of the volcanic pile. Characterization of the protolith depends on geochemical data for diagnostic elements that have not been mobilized, added, or removed. Established classification schemes using ratios of these stable elements indicate that the rocks were originally alkali basalts. This is the basalt type to be expected from the relatively small degrees of partial mantle melting induced by the early stages of continental rifting and basin development. The chemical composition is also typical of basalts generated within a continental setting. The continental setting and rift environment indicates that melting was initiated by decompression of the mantle under the actively extending basin rather than by a hot mantle plume.

Trace element ratios indicate that the sequence of basalt flows was not generated by differentiation (crystal fractionation) from a single parent magma. No geochemical evidence has been found for substantial fractionation of either olivine, chromite,

clinopyroxene, or plagioclase. The Audhild basalts show evidence of genesis by varying degrees of partial melting in an upper mantle source. A small amount (5% ?) of melting of a fertile garnet lherzolite source is indicated, and the basalts of the Audhild Formation represent the first melting of a fresh mantle. Considering the lack of fractionation, it appears that the Audhild volcanics were erupted before volumes of melt sufficient to establish large magma chambers had been produced beneath the developing Sverdrup Basin.

Tholeiitic dykes that intrude the Audhild Formation are not genetically linked to the volcanic sequence. Alkaline dykes may be later differentiates of the magma (or magmas) that produced the extrusive rocks, but this is not demonstrated with any certainty. Alkaline, transitional, and tholeiitic lavas were erupted in the Sverdrup Basin during the Permian magmatic phase (Cameron, in prep.) and in several episodes during the Cretaceous (Williamson, 1988). The dykes at Kleybolte Peninsula may be related to one or several of these episodes. Intrusive and extrusive activity was particularly voluminous during the Cretaceous, when large volumes of differentiated quartz tholeiites were erupted and emplaced (Williamson, 1988).

If the Audhild basalts are in fact primary mantle melts from an undepleted mantle source, they offer a rare opportunity to closely investigate mantle properties and processes, and are deserving of further study. A coordinated study of Carboniferous basalts at Clements Markham Inlet, on Axel Heiberg Island, and in the Audhild Formation would indicate whether conditions were

repeated at various locations within the Sverdrup Basin and whether the mantle source was uniform.

Further comparisons with later phases of Sverdrup Basin magmatism can be made by application of isotopic methods. A Nd/Sm isotope study would indicate the evolution of the mantle beneath the developing basin, but Sr isotope work might not be feasible in view of the extensive alteration in Paleozoic basalts of the Sverdrup Basin (Trettin, 1988, Cameron, in prep., this study).

The alteration and metamorphism of the Audhild volcanics (and of the other basalt occurrences) can be investigated by stable isotope methods. Such a study might indicate the source and nature of the fluids that promoted or induced chemical and mineralogical changes.

REFERENCES

Allegre, C.J. and Minster, J.-F. 1978. Quantitative models of trace element behaviour in magmatic processes. Earth and Planetary Science Letters 38, 1-25.

Allegre, C.J., Treuil, M, Minster, J.-F., Minster, B., Albarade, F. 1977. Systematic use of trace elements in igneous processes, Part I: Fractional crystallization processes in volcanic suites. Contributions to Mineralogy and Petrology 60, 57-75.

Balkwill, H.R. 1978. Evolution of Sverdrup Basin. American Association of Petroleum Geologists Bulletin 62, 1004-1028.

Balkwill, H.R., Cook, D.G., Detterman, R.L., Embry, A.F., Hakansson, E., Miall, A.D., Poulton, T.P. and Young, F.G. 1983. Arctic North America and Northern Greenland in The Phanerozoic Geology of the World, II The Mesozoic B. Elsevier Science Publishers, 1-31.

Basaltic Volcanism Study Project. 1981. Basaltic Volcanism on the Terrestrial Planets. Pergamon Press Inc., New York.

Best, M.G. 1982. Igneous and Metamorphic Petrology. W.H. Freeman and Company, New York.

Cameron, B. Masters Thesis in Progress, Dalhousie University, Halifax, Nova Scotia.

Deer, W.A., Howie, R.A., Zussman, J. 1962. Rock Forming Minerals, Vol. 1: Ortho- and Ring Silicates. Longmans, Green and Co. Ltd., London.

Deer, W.A., Howie, R.A., Zussman, J. 1963. Rock Forming Minerals, Vol. 2: Chain Silicates. Longmans, Green and Co. Ltd., London.

Duchesne, J.-C. 1983. The Lanthanides as Geochemical Tracers of Igneous Processes: An Introduction in Systematics and the Properties of the Lanthanides, S.P. Sinha ed. D. Reidel Publishing Company, Holland.

Geological Society of America. 1983. Decade of North American Geology, Geologic Time Scale.

Green, D.H. and Ringwood, A.E. 1967. The genesis of basaltic magmas. Contributions to Mineralogy and Petrology 15, 103-190.

Leterrier, J., Maury, R.C., Thonon, P., Girard, D. and Marchal, M. 1982. Clinopyroxene composition as a method of

identification of the magmatic affinities of paleo-volcanic series. Earth and Planetary Science Letters 59, 139-154.

MacDonald, G.A. and Katsura, T. 1964. Chemical composition of Hawaiian lavas. Journal of Petrology, 5, 82-133.

McKenzie, D. 1978. Some remarks on the development of sedimentary basins. Earth and Planetary Science Letters 40, 25-32.

McKenzie, D. 1984. A possible mechanism for epirogenic uplift. Nature 303, 919-618. .

McKenzie, D. and Bickle, M.J. 1988. The volume and composition of melt generated by extension of the lithosphere. Journal Of Petrology 29, 625-680.

Meschede, M. 1986. A method of discriminating between different types of mid-ocean ridge basalts and continental tholeiites with the Nb-Zr-Y diagram. Chemical Geology. 56, 207-218.

Minster, J.-F, and Allegre, C.J. 1978. Systematic use of trace elements in igneous processes, Part III: Inverse problem of batch partial melting in volcanic suites. Contributions to Mineralogy and Petrology 68, 37-52.

Muecke, G.K. 1983. Behaviour of the Rare Earth Elements during alteration and metamorphic processes; in Systematics and the Properties of the Lanthanides, S.P. Sinha ed. D. Reidel Publishing Company, Holland.

Pearce, J.A. and Cann, J.R. 1973. Tectonic setting of basic volcanic rocks determined using trace element analysis. Earth and Planetary Science Letters 19, 290-300.

Pearce, J.A. and Norry, M.J. 1979. Petrogenetic implications of Ti, Zr, Y and Nb variations in volcanic rocks. Contributions to Mineralogy and Petrology 69, 33-47.

Stephenson, R.A., Embry, A.F., Nakiboglu, S.M. and Hastaoglu, M.A. 1987. Rift-initiated Permian to Early Cretaceous subsidence of the Sverdrup Basin; in Sedimentary Basins and Basin-Forming Mechanisms, C. Beaumont and A.J. Tankard eds. Canadian Society of Petroleum Geologists Memoir 12, 213-231.

Takahashi, E. 1986. Melting of a dry peridotite KLB-1 up to 14GPa: implications on the origin of peridotitic upper mantle. Journal of Geophysical Research 91, 9367-9382.

Taylor, S.R. and McLennan, S.M. 1985. The Continental Crust: its Composition and Evolution. Blackwell Scientific Publications, Oxford.

Thorsteinsson, R. 1974. Carboniferous and Permian stratigraphy of Axel Heiberg Island and western Ellesmere Island, Canadian Arctic Archipelago. Geological Survey of

Canada Bulletin 224, 115p.

Thorsteinsson, R. and Trettin, H.P. 1970. Geology, Cape Stallworthy, District of Franklin: Geological Survey of Canada map 1305a.

Trettin, H.P. 1973. Early Paleozoic evolution of northern parts of Canadian Arctic Archipelago; in Arctic Geology, M.G. Pitcher ed. American Association of Petroleum Geologists, Memoir 19, 57-75.

Trettin, H.P. 1987. Investigations of Paleozoic geology, northern Axel Heiberg and northwestern Ellesmere islands; in Current Research, Part A, Geological Survey of Canada, Paper 87-1A, 357-367.

Trettin, H.P. 1988. Early Namurian (or older) alkali basalt in the Borup Fiord Formation, northern Axel Heiberg Island in Current Research, Geological Survey of Canada, Paper 88-1.

Williamson, M.-C. 1988. The Cretaceous Igneous Province of the Sverdrup Basin, Canadian Arctic: Field Relations and Petrochemical Studies. Ph.D. Thesis, Dalhousie University, Halifax, Nova Scotia.

Winchester, J.A. and Floyd, P.A. 1977. Geochemical discrimination of different magma series and their products using immobile elements. Chemical Geology, 20, 325-343.

Plate 1. View looking NE from Bjare Strait to coastal outcrop of Audhild Formation. Recessive Emma Fiord Formation and Borup Fiord Formation are at left.

Plate 2. Bedded sequence of basalt lapilli, pumice (white), ash (maroon), and rare clastic pebbles near 15 m in measured section.

Plate 3. Poorly bedded sequence of basalt lapilli, pumice, and ash; coarsens upward (stratigraphic top at left of photo). Near 20 m in measured section.

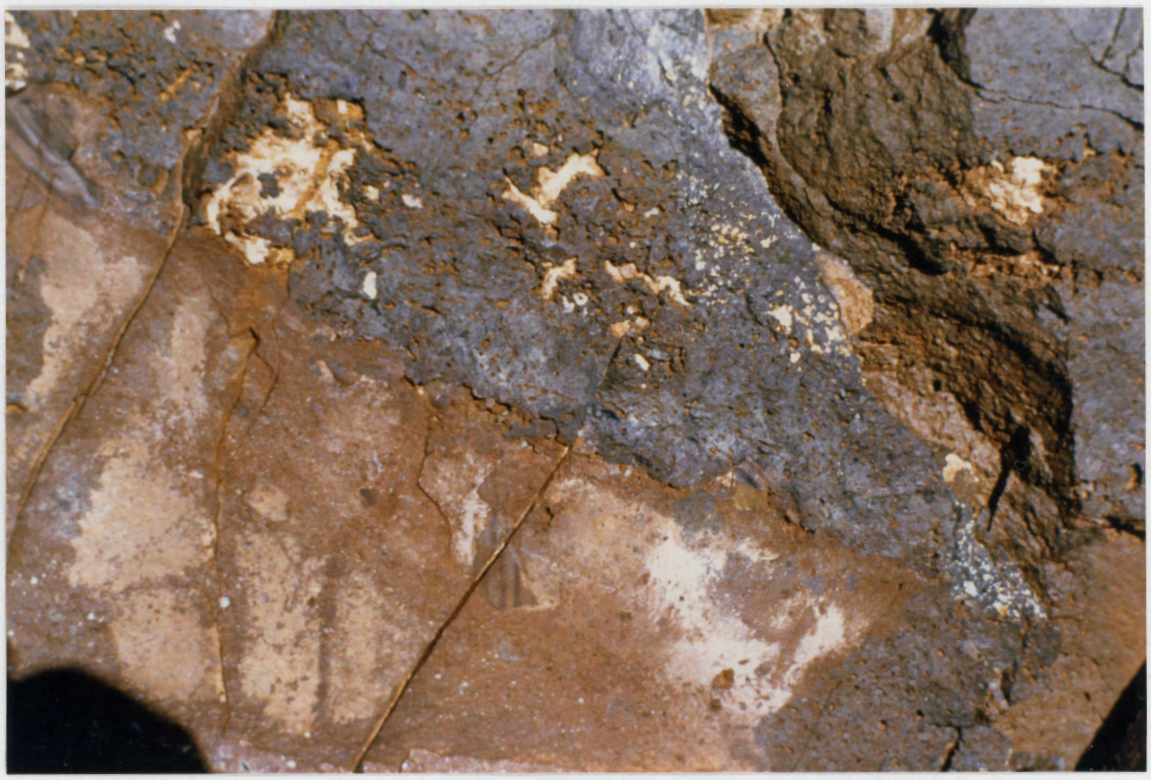

Plate 4. Amygdaloidal flow base above sediment horizon; at 38 m in measured section. Maximum field of view ~ 70 cm.

Plate 5. Rubbly amygdaloidal flow top overlain by maroon sediment horizon; at 37.5 m in measured section. Maximum field of view ~ 60 cm.

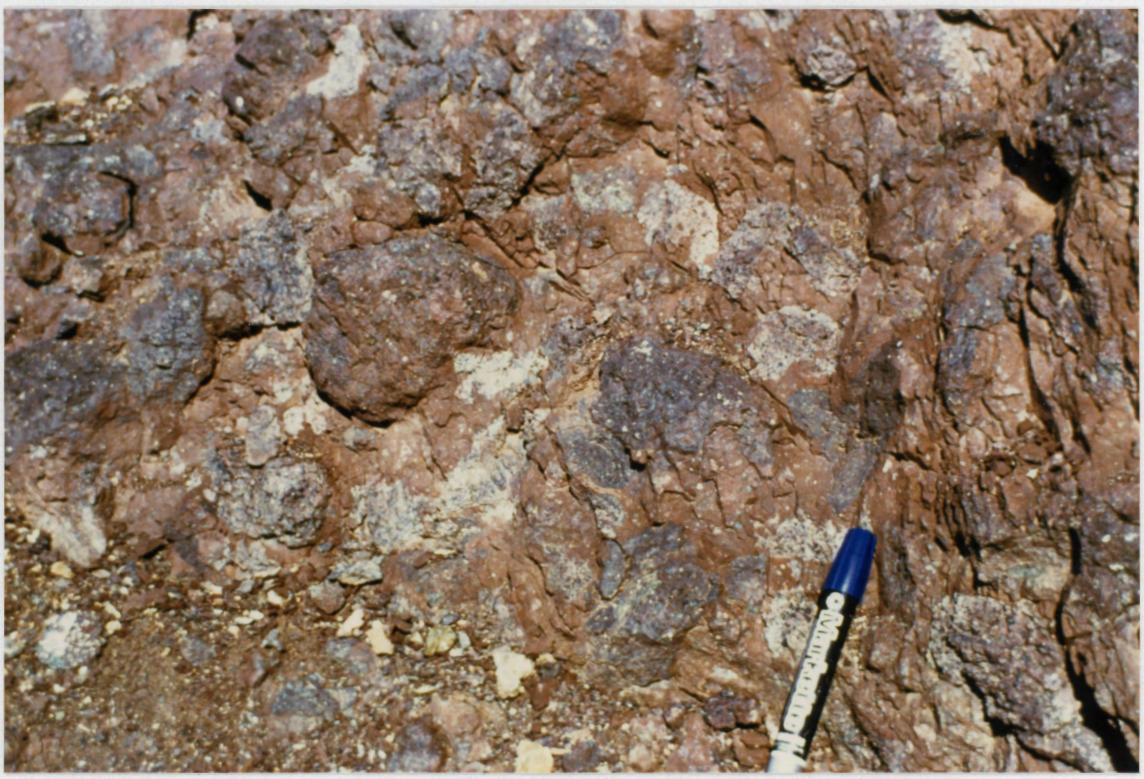

Plate 6. Unbedded matrix supported conglomerate with amygdaloidal basalt cobbles. Near 105 m in measured section.

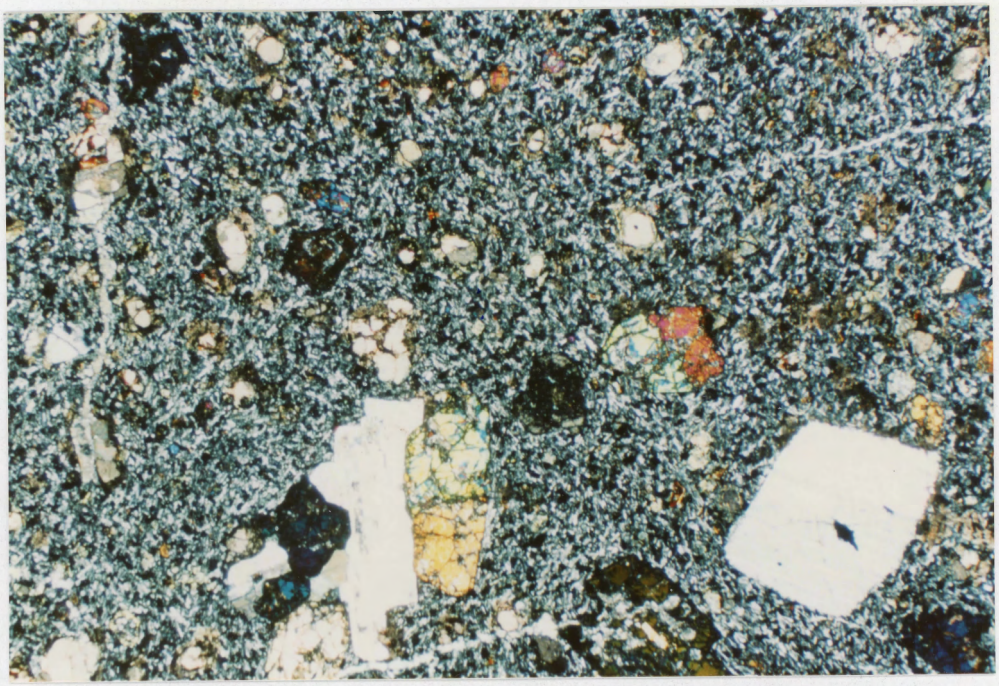

Plate 7. Glomerocrysts and phenocrysts of plagioclase and pyroxene in EL 87-176 (Flow). XN, 12 x 9 mm.

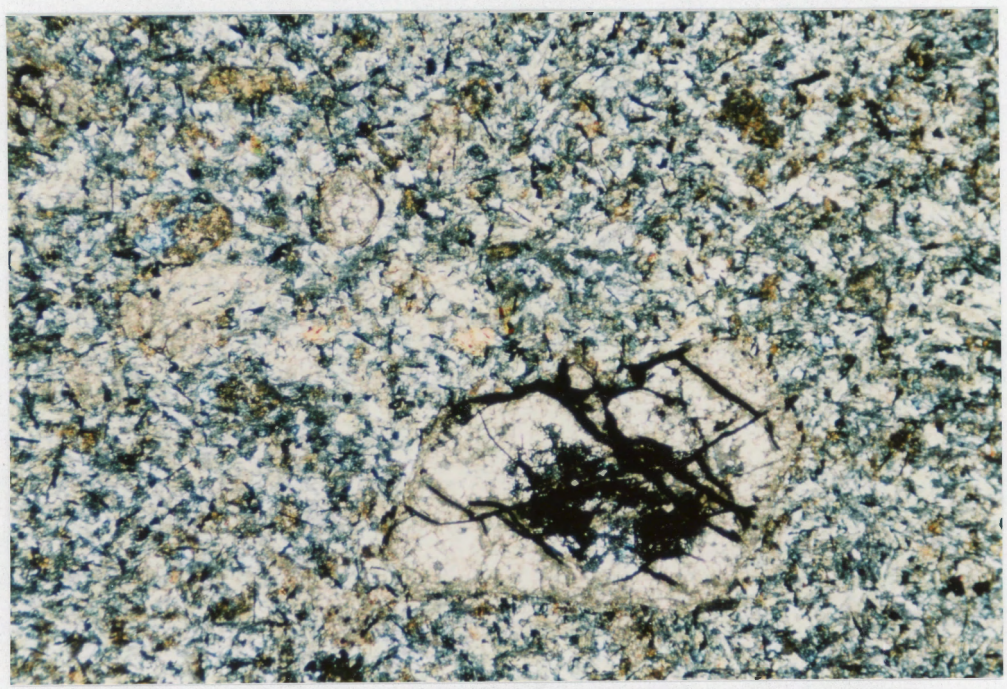

Plate 8. Highly altered basalt flow (EL 87-166) with relict ferromagnesian phenocryst. XN, 6 x 4.5 mm.

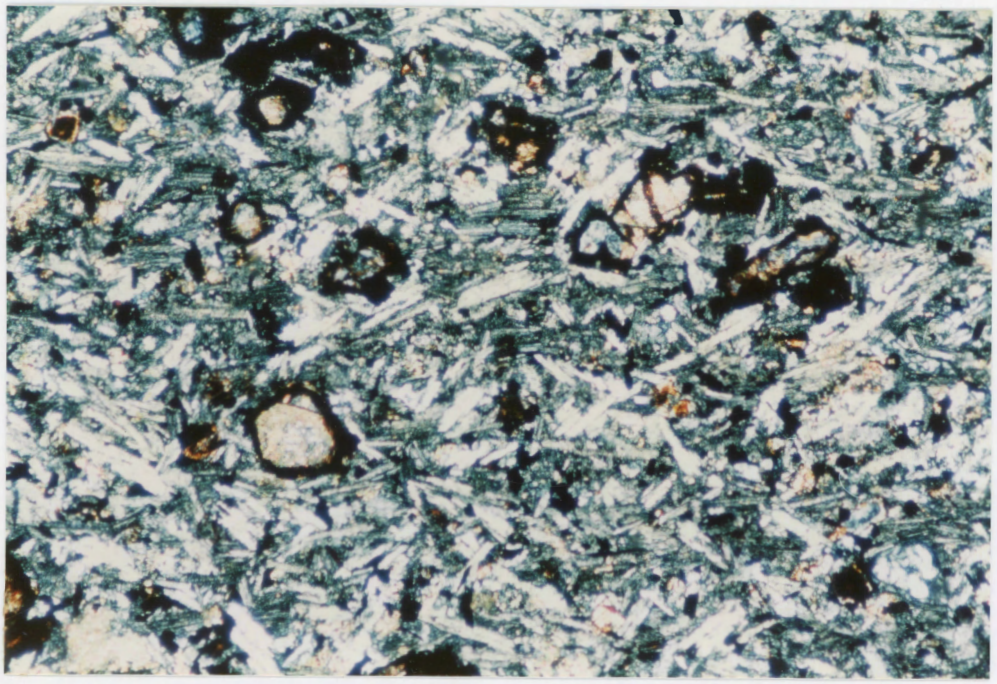

Plate 9. Flow texture defined by aligned plagioclase laths in EL 87-169. XN, 3 x 2 mm.

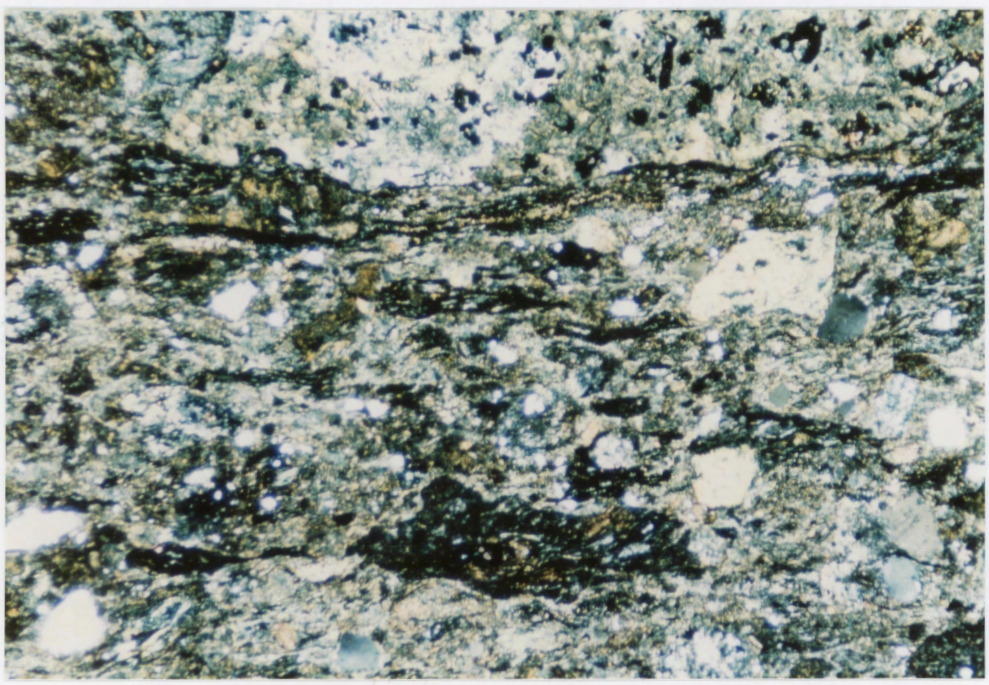

Plate 10. Fragmental texture of pumice and quartz clasts in EL 87-158 (Pyroclastic). XN, 6 x 4.5 mm.

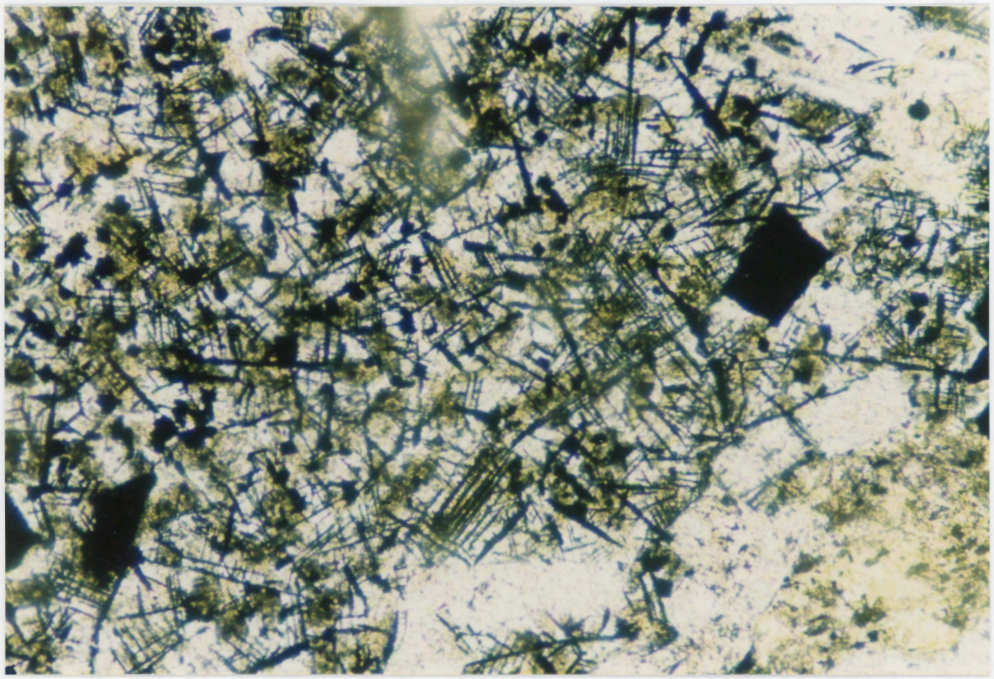

Plate 11. Blocky and acicular opaque grains in EL 87-172 (Dyke). PPL, 1.2 x 0.8 mm.

Plate 12. Granular to subophitic texture in basaltic dyke (EL 87-157). XN, 6 x 4.5 mm.

Plate 13. EL 87-160 (Plagioclase-porphyry dyke) with aggregate of chlorite and calcite (green-white) near centre of photo. Also dark pyroxene in groundmass and sericitized plagioclase phenocrysts. PPL, 12 x 9 mm.

Plate 14. Highly altered basalt flow (EL 87-175) with secondary opaque mineral as a cavity filling phase and abundant chlorite (blue) in groundmass. XN, 12 x 9 mm.

APPENDIX A Petrography

EL-87-157

Sparsely plagioclase phyric basaltic dyke with granular to sub-ophitic texture; slightly altered.

1% intensely sericitized plagioclase phenocrysts up to 5mm
40% clinopyroxene, mostly interstitial
40% plagioclase laths to 0.5mm
10% subangular opaque grains
2% chlorite in groundmass
minor patches of alteration products

EL-87-158

Graded bed of pyroclastics/volcaniclastics with compositional on a scale of ~2mm; moderately to highly altered.

30% pumice fragments, composed of sericite and opaque minerals
10% quartz grains
20 "dusty" opaques, <.05mm
5% sericitized plagioclase up to 1mm

EL-87-159

Basaltic dyke displaying inequigranular to slightly porphyritic texture dominated by plagioclase and clinopyroxene; slightly altered.

25% clinopyroxene up to 1mm (subphenocryst size)
40% plagioclase laths seriate size distribution 0.2 - 2mm
20% fine grained alteration products (after olivine or other ferromagnesian?)
10% blocky, subangular opaques
5% brown amphibole as discrete grains >0.05mm

EL-87-160

Plag-Porphyry Dyke; highly porphyritic and moderately altered.

35-40% Subhedral plagioclase phenocrysts up to 7mm, ~40 to 90% replaced by sericite
20% ragged brown pyroxenes in groundmass up to 0.6mm
20% sericitized plag laths up to 0.3mm
10% granular opaques up to 0.6mm but rarely >0.1mm
10% chlorite and calcite (pseudomorphs of olivine?) up to 3mm

EL-87-161

Sparsely plag phyric dyke with inequigranular to sub-ophitic texture in groundmass; moderately altered.

1% plagioclase phenocrysts with sericitized cores
40% clinopyroxene up to 1.5mm, some is interstitial to plagioclase
30% sericitized plagioclase laths 0.2 - 2mm
20% granular opaques 0.1mm
10% brown and green chlorite

EL-87-162
Fine grained inequigranular basaltic dyke; moderately altered.
50% subhedral plagioclase, moderately sericitized stubby laths up to 0.6mm
15% anhedral clinopyroxene; slightly clouded, 0.2 - 0.5mm
15-20% blocky opaque grains 0.2mm; some acicular to 0.5mm
15% chlorite, mostly as discrete,distinct patches 0.2mm

EL-87-163
Glomeroporphyritic amygdaloidal basalt; moderately altered.
5% glomerocrysts of plagioclase, 5m
50% Moderately sericitized plagioclase laths in groundmass, 0.2mm
10% polygonal chlorite pseudomorphs, 0.2mm
15% interstitial chlorite in groundmass, 0.2mm
10% granular opaques, 0.1mm (primary)
2% "dusty" opaques (secondary)
10% calcite in amygdales
2% zeolite in cores of amygdales

EL 87-164
Porphyritic basalt; moderately altered.
15% relict olivine phenocrysts replaced by calcite and opaque minerals
5% highly sericitized anhedral plagioclase phenocrysts, 3mm
35% clouded and sericitized plagioclase laths in groundmass, mm
10% granular opaques. mm
5% secondary opaques in groundmass
15% chlorite in groundmass
15% calcite in groundmass

El 87-165
Porphyritic basalt; highly altered.
15% pseudomorphs of oxides and calcite after olivine, 0.2 - 2mm
40% sericitized plagioclase laths
15% granular opaques
5% dusty opaques (secondary)
105 chlorite, interstitial between groundmass plagioclase and as discrete "pods" up to 0.5mm

El 87-166
Porphyritic basalt; highly altered.
10% calcite and opaque pseudomorphs of olivine
2% highly sericitized plagioclase phenocrysts, up to 3mm
50% groundmass plagioclase laths, 0.2mm
5% acicular opaques
5% granular opaques
20% chlorite in groundmass, often with 0.01mm inclusions of secondary opaque minerals
minor groundmass calcite
10% diffuse brown alteration products

EL 87-167
Glomeroporphyritic basalt; moderately altered.
10% calcite and opaque pseudomorphs of olivine phenocrysts, mm
5% sericitized plagioclase phenocrysts, mm
50% sericitized plagioclase in groundmass, mm
5% granular opaques up to 1mm; both primary and secondary
20% brown and green chlorite in groundmass, as distinct bodies up to 2mm (with opaque inclusions), and as a vug filling
minor groundmass calcite
minor brown and black "iddingsite"

El 87-168
Inequigranular to porphyritic basaltic dyke or sill; moderately altered.
10% fractured and clouded clinopyroxene up to 1.5mm
60% moderately sericitized plagioclase laths 0.2 - 2mm
10% acicular (skeletal) opaque mineral grains
5% anhedral and blocky opaque mineral grains
10% chlorite
5% dark, cloudy alteration products in association with groundmass minerals (mostly after cpx or olivine?)

EL 87-169
Porphyritic amygdaloidal basalt with evident flow texture; moderately altered.
15% relict olivine phenocrysts, replaced by calcite and opaque minerals
60% moderately sericitized plagioclase laths in groundmass
10% granular opaques 0.05 - 0.5mm; some may be secondary
10% calcite in filled vesicles
2% radiating aggregates of zeolite mineral in cores of amygdales
2% silica as vesicle and vug filling

El 87-170
Porphyritic basalt, with an evident flow fabric in groundmass; highly altered.
15% relict olivine phenocrysts, replaced by calcite and opaque minerals ("iddingsite")
40% sericitized and chloritized plagioclase laths ~0.1mm
10% anhedral opaque grains 0.05mm
15% brown and green chlorite, mostly as diffuse patches
2% silica as a vug or vesicle filling
3% fine grained calcite filling vugs and cavities 1x4mm aligned parallel to flow
5% calcite and opaques as fracture filling or veinlet
5% groundmass calcite

EL 87-171
Porphyritic basalt; moderately to highly altered.
15% relict olivine phenocrysts, replaced by calcite and opaque minerals ("iddingsite"), 0.2 - 1mm
40% sericitized and chloritized plagioclase laths
10% anhedral opaque grains 0.05mm
15-20% brown and green chlorite, mostly diffuse patches in groundmass but some associated with calcite as a vug filling
10% calcite as vein, vug, and vesicle filling
5% silica in vugs or amygdales, euhedral/subhedral along rim with fine grained calcite, anhedral at core with coarse calcite

EL 87-172
Porphyritic basaltic dyke; moderately altered.
10% sericitized plagioclase phenocrysts, 1 -2mm
5% highly altered and replaced clinopyroxene phenocrysts, 2mm
5% blocky opaque grains, 0.2mm
10% acicular opaque minerals in groundmass, 0.2mm
5% blocky opaque minerals in groundmass, 0.02mm
35% anhedral sericitized plagioclase in groundmass
15-20% patchy chlorite and other alteration products in groundmass
10-15% chlorite "pods" or replaced minerals of phenocryst size

EL 87-173
Inequigranular to seriate basaltic dyke; moderately altered.
50% clouded and slightly chloritized anhedral plagioclase, nearly continuous size distribution from 0.2 - 1.5mm
20% clouded and fractured clinopyroxene partly replaced by chlorite and opaque minerals, 0.1 - 1.5mm
15% granular opaque minerals 0.1mm
15% brown and green chlorite, mostly as distinct "grains" or replacement bodies, rare diffuse replacement

EL 87-174
Porphyritic basalt; highly altered
15% euhedral plagioclase phenocrysts, slightly chloritized and sericitized, 0.5 - 1.5mm
10% relict olivine phenocrysts replaced by calcite, opaques, and chlorite, 0.5 - 1mm
35% sericitized plagioclase in groundmass, 0.1 - 0.2mm
10% acicular and blocky opaque minerals (some are secondary)
15% calcite in filled vugs and vesicles
minor calcite in groundmass
10-15% chlorite in groundmass and in association with calcite fillings

EL 87-175

Porphyritic basalt; moderately to highly altered.
5% slightly sericitized euhedral plagioclase phenocrysts up to 3mm
5% relict olivine phenocrysts replaced by calcite and opaques
10-15% acicular and blocky opaque minerals (some are secondary)
35% sericitized plagioclase in groundmass, 0.1 - 0.5mm
10% calcite in veins and filled vugs and vesicles
15-20% chlorite, mostly in groundmass, but also common in rims of amygdales, at core of an irregular vug and in veinlet with calcite
5% granular quartz in groundmass and with other secondary minerals in vugs and vesicles
5% radiating aggregates of low birefringence zeolite minerals in amygdales with quartz and calcite; also as a groundmass replacement mineral in association with quartz

EL 87-176

Porphyritic basalt; slightly altered.
10% anhedral to subhedral clinopyroxene phenocrysts, 2 - 3mm
5% slightly sericitized subhedral plagioclase phenocrysts, 2-4mm
5% relict olivine phenocrysts replaced by calcite, opaques, and chlorite
15% blocky or irregular opaque grains
30% moderately sericitized and chloritized plagioclase laths in groundmass, 0.2mm
30% chlorite, interstitial and after groundmass plagioclase, also with calcite in veinlets and as a fibrous aggregate in several fillings or replacements ~3mm
minor brown amphibole
minor calcite in veinlets

EL 87-177

Porphyritic basalt; highly altered.
15% relict olivine phenocrysts replaced by calcite, opaques ("iddingsite"), and chlorite, 1 - 2mm
25-30% plagioclase laths in groundmass, 0.1 - 0.2mm
15% blocky and irregular opaque grains (some probably secondary)
20% groundmass calcite
5% calcite in vugs
5% silica in vugs
10% chlorite, mostly after olivine, some in groundmass (heterogeneous distribution, with some chloritized zones or areas)

EL 87-178

Porphyritic basalt; highly altered.

15% relict olivine phenocrysts replaced by calcite, opaques, and chlorite, 1 - 2mm

30% plagioclase laths in groundmass, 0.1 - 0.2mm

15% anhedral opaque grains (some secondary)

10% calcite in amygdales and veins

10% groundmass calcite

5% silica in amygdales

10% chlorite in veins with calcite and in groundmass

5% patchy brown alteration minerals and "iddingsite"

APPENDIX B : Mean Clinopyroxene Analyses

	EL87-157 (8)	EL87-159 (8)	EL87-160 (7)	EL87-161 (12)	EL87-162 (4)
SiO2	50.19	46.65	44.27	51.00	49.25
TiO2	0.89	2.71	4.21	0.78	1.49
Al2O3	2.82	6.25	7.62	2.65	4.03
Cr2O3	0.16	0.07	0.01	0.25	0.04
FeO	9.64	8.78	10.15	9.52	10.81
MnO	0.23	0.21	0.19	0.21	0.23
MgO	15.69	13.19	11.14	15.96	14.28
CaO	18.76	21.10	22.42	19.38	19.48
Na2O	0.28	0.55	0.59	0.29	0.38
Total	98.66	99.53	100.58	100.05	99.99
Si	0.316	0.294	0.280	0.317	0.308
Ti	0.004	0.013	0.020	0.004	0.007
Al	0.021	0.046	0.057	0.019	0.030
Cr	0.001	0.000	0.000	0.001	0.000
Fe	0.051	0.046	0.054	0.050	0.057
Mn	0.001	0.001	0.001	0.001	0.001
Mg	0.147	0.124	0.105	0.147	0.133
Ca	0.126	0.142	0.152	0.129	0.131
Na	0.003	0.007	0.007	0.004	0.005
Sum O	2.64	2.64	2.63	2.68	2.66

	EL87-168 (8)	EL87-172 (2)	EL87-173 (11)	EL87-176 (15)
SiO2	49.58	49.82	48.86	50.19
TiO2	1.45	1.78	1.99	1.40
Al2O3	3.78	3.71	4.04	4.58
Cr2O3	0.05	0.06	0.05	0.25
FeO	10.46	10.40	9.46	7.59
MnO	0.23	0.30	0.28	0.19
MgO	15.36	14.28	14.22	15.43
CaO	18.91	19.17	20.54	20.20
Na2O	0.36	0.36	0.44	0.52
Total	100.18	99.90	99.93	100.36
Si	0.309	0.311	0.306	0.309
Ti	0.007	0.008	0.009	0.006
Al	0.028	0.027	0.030	0.033
Cr	0.000	0.000	0.000	0.001
Fe	0.055	0.054	0.050	0.039
Mn	0.001	0.002	0.001	0.001
Mg	0.143	0.133	0.133	0.141
Ca	0.126	0.128	0.138	0.133
Na	0.004	0.004	0.005	0.006
Sum O	2.67	2.66	2.66	2.70

Appendix C: Whole Rock Geochemistry

Table C1 - Major and Minor Element Oxides and Loss on Ignition (wt %), XRF and INAA Trace Elements (ppm)

	EL87-157	EL87-158	EL87-159	EL87-160	EL87-161
SiO_2	49.39	51.05	44.68	46.45	49.47
Al_2O_3	13.43	19.37	13.60	21.37	13.51
Fe_2O_3	12.89	9.06	12.73	8.25	12.86
MgO	6.30	5.17	5.49	3.91	6.51
CaO	10.43	0.95	11.00	8.62	10.81
Na_2O	2.36	0.93	3.14	2.84	2.15
K_2O	0.73	5.90	1.10	3.58	0.54
TiO_2	2.04	3.12	3.67	1.74	2.01
MnO	0.20	0.04	0.19	0.11	0.19
P_2O_5	0.20	0.32	0.67	0.35	0.20
L.O.I.	0.70	4.30	4.10	2.80	0.50
TOTAL	98.68	100.14	100.43	100.29	98.81
Ba	118	925	538	669	91
Rb	20	130	21	62	14
Sr	249	74	609	1064	236
Y	28	23	28	15	29
Zr	145	302	210	164	145
Nb	11	63	46	28	13
Th	.	.	.	.	.
Pb	.	.	.	.	.
Ga	22	23	19	21	20
Zn	94	32	105	67	92
Cu	182	.	23	9	185
Ni	74	250	21	14	73
V	385	318	350	194	386
Cr	121	309	.	16	115
Sc	41.4	-	-	17.4	40.8
Hf	3.60	-	-	2.74	3.68
Th	1.22	-	-	2.26	1.10
Ta	1.02	-	-	2.00	0.98
Co	56.0	-	-	35.4	56.3
La	10.3	-	-	20.9	10.3
Ce	26.1	-	-	44.1	25.5
Nd	17.2	-	-	21.8	16.8
Sm	4.68	-	-	4.69	4.84
Eu	1.68	-	-	1.65	1.63
Tb	0.86	-	-	0.54	0.84
Yb	2.86	-	-	1.38	2.93
Lu	0.48	-	-	0.22	0.49

Table C1 Continued

	EL87-162	EL87-163	EL87-164	EL87-165	EL87-166
SiO_2	49.29	41.35	43.89	43.94	48.62
Al_2O_3	13.10	13.60	12.86	13.08	14.98
Fe_2O_3	14.08	9.81	12.08	10.14	6.83
MgO	5.00	7.44	7.66	4.55	5.06
CaO	5.93	11.33	8.01	12.29	8.89
Na_2O	4.49	4.03	3.05	4.06	4.67
K_2O	1.03	0.28	1.11	0.49	1.07
TiO_2	3.52	2.11	2.15	2.10	1.93
MnO	0.19	0.11	0.12	0.14	0.11
P_2O_5	0.47	0.45	0.46	0.27	0.34
L.O.I.	1.90	10.60	9.40	10.00	8.20
TOTAL	99.15	101.14	100.96	101.05	100.65
Ba	227	135	84	64	195
Rb	24	8	24	14	21
Sr	310	169	112	202	245
Y	37	20	23	19	22
Zr	259	227	212	134	218
Nb	27	51	53	26	39
Th	.	15	.	.	.
Pb	.	.	.	.	.
Ga	21	19	16	19	18
Zn	129	40	91	74	76
Cu	36	13	.	.	.
Ni	29	250	236	357	186
V	422	216	213	213	183
Cr	22	555	481	416	393
Sc	-	-	-	-	21.9
Hf	-	-	-	-	5.24
Th	-	-	-	-	5.96
Ta	-	-	-	-	3.45
Co	-	-	-	-	44.9
La	-	-	-	-	29.0
Ce	-	-	-	-	58.8
Nd	-	-	-	-	27.7
Sm	-	-	-	-	5.44
Eu	-	-	-	-	1.47
Tb	-	-	-	-	0.73
Yb	-	-	-	-	1.99
Lu	-	-	-	-	0.33

Table C1 Continued

	EL87-167	EL87-168	EL87-169	EL87-170	EL87-171
SiO_2	46.98	49.00	47.67	47.66	49.40
Al_2O_3	14.17	12.99	12.86	13.90	12.46
Fe_2O_3	11.57	13.74	12.87	9.11	10.29
MgO	4.89	4.91	5.56	6.15	6.89
CaO	7.44	5.25	6.60	7.91	6.05
Na_2O	5.22	2.88	3.21	4.86	3.27
K_2O	1.36	3.53	1.93	0.65	2.60
TiO_2	1.81	3.43	2.25	2.50	2.16
MnO	0.11	0.27	0.10	0.12	0.11
P_2O_5	0.33	0.47	0.37	0.45	0.42
L.O.I.	7.20	1.90	7.30	7.90	7.10
TOTAL	101.09	98.50	100.74	101.09	100.87
Ba	347	1076	495	137	495
Rb	12	78	26	13	40
Sr	136	393	187	205	243
Y	25	43	22	24	23
Zr	203	268	205	235	210
Nb	37	27	42	51	44
Th	.	.	.	10	.
Pb	.	.	.	.	.
Ga	19	23	19	18	16
Zn	56	146	64	159	75
Cu	.	28	.	.	.
Ni	210	25	201	181	180
V	182	408	266	264	220
Cr	401	15	408	378	334
Sc	21.0	29.2	21.9	-	-
Hf	5.10	6.91	5.06	-	-
Th	5.82	5.31	5.08	-	-
Ta	3.24	2.28	3.57	-	-
Co	29.7	47.9	33.6	-	-
La	28.8	31.9	36.8	-	-
Ce	59.1	73.5	74.5	-	-
Nd	27.0	41.4	31.3	-	-
Sm	5.75	9.08	6.13	-	-
Eu	1.84	2.72	1.91	-	-
Tb	0.78	1.35	0.81	-	-
Yb	1.98	3.56	1.67	-	-
Lu	0.30	0.57	0.25	-	-

Table C1 Continued

	EL87-172	EL878-173	EL87-174	EL87-175	EL87-176
SiO_2	46.47	47.79	49.37	51.72	47.42
Al_2O_3	13.66	13.96	14.57	13.96	13.69
Fe_2O_3	13.61	12.49	4.75	9.36	8.85
MgO	4.90	4.16	4.61	4.52	7.91
CaO	5.21	7.32	10.44	8.17	9.30
Na_2O	3.30	3.11	4.53	2.65	2.60
K_2O	3.59	2.86	2.08	1.20	1.89
TiO_2	3.77	3.05	2.16	2.12	2.06
MnO	0.27	0.19	0.10	0.09	0.11
P_2O_5	0.50	1.16	0.39	0.36	0.41
L.O.I.	4.40	2.30	8.00	6.10	5.70
TOTAL	99.67	98.75	101.01	100.34	100.42
Ba	1489	702	188	235	489
Rb	61	56	26	22	47
Sr	328	1182	271	367	483
Y	38	35	22	18	25
Zr	267	301	202	192	237
Nb	27	46	36	34	42
Th	.	12	.	.	.
Pb	.	.	.	.	.
Ga	24	19	17	19	21
Zn	129	123	53	59	94
Cu	52	7	.	34	.
Ni	29	13	209	203	230
V	475	230	217	192	207
Cr	27	.	342	326	316
Sc	-	-	-	21.9	24.3
Hf	-	-	-	4.61	5.53
Th	-	-	-	3.56	4.32
Ta	-	-	-	2.66	3.52
Co	-	-	-	35.6	51.3
La	-	-	-	23.4	32.8
Ce	-	-	-	49.7	66.7
Nd	-	-		24.3	30.6
Sm	-	-	-	5.32	6.94
Eu	-	-	-	1.74	2.12
Tb	-	-	-	0.73	0.81
Yb	-	-	-	1.81	1.87
Lu	-	-	-	0.29	0.28

Table C1 Continued

	EL87-177	EL87-165(dup)	EL87-171(dup)
SiO_2	45.12	43.91	49.51
Al_2O_3	11.97	13.17	12.50
Fe_2O_3	8.90	10.11	10.39
MgO	5.86	4.62	6.57
CaO	11.26	12.27	5.97
Na_2O	4.15	4.20	3.06
K_2O	1.61	0.50	2.60
TiO_2	1.73	2.09	2.16
MnO	0.12	0.15	0.11
P_2O_5	0.27	0.27	0.41
L.O.I.	10.10	9.90	7.20
TOTAL	101.23	101.19	100.62
Ba	102	72	508
Rb	34	13	45
Sr	142	200	250
Y	20	18	23
Zr	169	135	209
Nb	40	23	44
Th	13	.	14
Pb	.	.	.
Ga	17	18	16
Zn	49	74	73
Cu	.	.	.
Ni	178	358	179
V	181	209	218
Cr	367	420	333
Sc	20.1	-	-
Hf	4.48	-	-
Th	8.06	-	-
Ta	3.90	-	-
Co	29.5	-	-
La	32.3	-	-
Ce	64.1	-	-
Nd	28.8	-	-
Sm	5.95	-	-
Eu	1.82	-	-
Tb	0.76	-	-
Yb	1.69	-	-
Lu	0.26	-	-

Notation: . = not detected during analysis
- = not analysed